Preprint version, Reference: Murano, A., Ortega, J., Vasconcelos, G., Rodrigues, H. Influence of traditional earthquake-resistant techniques on the out-of-plane behavior of stone masonry walls: experimental and numerical assessment. *Engineering Structures* (2020). https://doi.org/10.1016/j.engstruct.2019.109815

Influence of traditional earthquake-resistant techniques on the out-of-plane behaviour of stone masonry walls: experimental and numerical assessment

Antonio Murano[a], Javier Ortega[a*], Graça Vasconcelos[a], Hugo Rodrigues[b]

[a] ISISE, Department of Civil Engineering, University of Minho, Guimarães, Campus de Azurém, 4800-058 Guimarães, Portugal; antoniomurano1987@gmail.com (A. Murano); javier.ortega@civil.uminho.pt (J. Ortega); graca@civil.uminho.pt (G. Vasconcelos)

[b] RISCO, School of Technology and Management, Polytechnic Institute of Leiria, Campus 2, 2411-901 Leiria, Portugal; e.mail: hugo.f.rodrigues@ipleiria.pt (H. Rodrigues)

* Corresponding author; e-mail: javier.ortega@civil.uminho.pt

Abstract: The main goal of the work is to assess the efficiency of traditional earthquake resistant solutions to improve the out-of-plane performance of stone masonry walls. Therefore, the present paper presents the results of an experimental campaign and numerical analysis performed on three stone masonry walls with a U-shaped plan configuration. Two of them were built with traditional earthquake-resistant techniques usually found in European Mediterranean area, namely steel ties and timber-laced reinforcements embedded at the corners of the walls. These techniques are specifically intended to enhance wall-to-wall connections and, thus, improve the out-of-plane behaviour of the walls. The experimental campaign included qualitative assessment procedures, non-destructive tests for the material characterization and a quasi-static test for the characterization of the out-of-plane response. Additionally, a finite element numerical model was built, calibrated with the experimental results, allowing to perform a parametric study to evaluate the influence of the number of reinforcements and geometrical configuration on the out-of-plane behaviour of stone masonry walls.

Keywords: stone masonry; vernacular architecture; earthquake resistant techniques; out-of-plane test; seismic assessment; masonry quality index; non-destructive tests; experimental analysis; finite element analysis; parametric study

Preprint version, Reference: Murano, A., Ortega, J., Vasconcelos, G., Rodrigues, H. Influence of traditional earthquake-resistant techniques on the out-of-plane behavior of stone masonry walls: experimental and numerical assessment. *Engineering Structures* (2020). https://doi.org/10.1016/j.engstruct.2019.109815

1. Introduction

Stone masonry is a traditional construction material widely used in the building practice throughout history. Historical stone masonry buildings have a considerable resistance to static vertical loads. Nevertheless, earthquakes represent one of the major threats to these structures. Common construction details typically observed in this type of structures (e.g. high percentage of voids, lack of effective connections among structural components, irregular arrangement of the masonry units, low quality materials) can negatively affect the seismic behaviour of stone masonry constructions and eventually lead to out-of-plane failures in the event of an earthquake.

This work aims at contributing to the better understanding of the out-of-plane behaviour of stone masonry walls, as well as assessing the efficiency of using traditional earthquake resistant solutions to improve it. Two traditional earthquake resistant techniques largely widespread in Mediterranean region [1], namely steel ties and timber-laced reinforcements, are herein analysed.

Vernacular architecture is a consistent and valuable part of the built-up environment to be preserved. It relies on an empirical approach and reflects the cultural and construction tradition of a community, as well as its bond with the natural environment [2]. As part of its close bond with the natural environment, vernacular architecture also shows signs of adaptation to natural hazards, such as earthquakes. This is the essence of the so-called “local seismic culture” of traditional communities. Local seismic culture is often founded on ergonomic considerations rather than economic principles and aims at minimizing the disadvantages and maximizing the advantages of a specific natural and social environment [3].

Some of the most significant examples of vernacular architecture combined with local seismic culture can be found in countries such as Portugal [4], Italy [5], Greece [6] and Turkey [7]. In order to fully take advantage of the dissipation capability of a structure, most of these techniques are intended to enhance its box behaviour. With that purpose, tying/anchoring systems and rigid floor diaphragms are used to improve the connection of separated walls in seismic upgrading interventions on existing buildings [8].

1.1. Experimental and numerical approaches

In the recent years, experimental works have been made concerning the out-of-plane seismic behaviour of masonry elements using laboratory or in situ tests [9]. In 1992, Ceradini [2] carried out one of the first attempt to study the behaviour of masonry structures subjected to out-of-plane horizontal loading actions. An inclinable supporting plane, inducing different levels of out-of-plane loading, was used to test masonry walls prototypes. Most recently, shaking table tests assessing the out-of-plane response of unreinforced masonry walls have been carried out by different authors, such as Doherty [10], D'Ayala [11] and Al Shawa [12]. The main aspects under studying in these experimental campaigns relate to the influence of the slenderness ratio and masonry bond arrangement on the overall seismic performances of the masonry panels. With similar purposes, more complex prototypes were tested in the shaking table at LNEC in Lisbon by Costa et al. [13] and Candeias [14]. Additionally, within the framework of the project "Study of the vulnerability of masonry buildings in Groningen", two bi-directional (horizontal and vertical) shake table tests were performed by Tomassetti [15] and Graziotti [16] in order to assess the seismic vulnerability of typical Dutch unreinforced masonry buildings exposed to small magnitude seismic events induced by reservoir depletion due to natural gas extraction.

Regarding experimental quasi-static tests, several examples can be found in Ferreira [17] and Dizhur [18]. Vakulik [19] carried out shaking table tests on half-scale two-way spanning unreinforced masonry walls (clay bricks walls) obtaining a good agreement with previous quasi-static tests [20] in terms of peak load, stiffness/strength degradation and damage patterns. Maccarini [21] also carried out an experimental campaign aiming at the characterization of the out-of-plane behaviour of unreinforced stone masonry walls at the University of Minho (Portugal).

With respect to the numerical simulation of the seismic behaviour of masonry structures, one of the main challenges is the use of adequate constitutive materials models, which allow reproducing its non-linear behaviour. Masonry mechanical properties highly depend on the overall quality and arrangement of both masonry units and mortar layers. Due to its extremely diversified nature, different numerical techniques have been developed by researchers over time, in order to deal with the complex task of modelling masonry structures [22]. Equivalent continuum idealization (macro-modelling) and equivalent discontinuous idealization (micro-modelling and meso-modelling) are the main FE-based approaches that have been used to model masonry as a composite material [9] [23]. Macro-modelling provides a good solution when a balance between accuracy and efficiency is required and is the approach selected to study the out-of-plane behaviour of stone masonry walls in the present work.

1.2. Objective and methodology of the present work

The present work represents an extension of the abovementioned experimental campaign carried out by Maccarini [21] and aims at evaluating the influence of different earthquake resisting techniques on the out-of-plane behaviour of stone masonry walls, namely: (1) steel ties (Wall_Stl); and (2) timber-laced reinforcements (Wall_Tmb). The results obtained are systematically compared with the unreinforced wall (Wall_Ref) tested by Maccarini [21], taking into account that the same geometry for the walls, testing setup and instrumentation were adopted. The research methodology relies on the combination of experimental and numerical research, regarded as complementary activities for an improved and comprehensive characterization of the stone masonry walls.

The experimental work includes non-destructive testing of the two stone masonry walls for the material and structural characterization, by means of sonic tests and dynamic identification tests for the preliminary prediction of elastic properties of stone masonry. Sonic tests aim primarily at estimating the elastic properties of masonry, namely the modulus of elasticity (E). Dynamic identification tests were intended to obtain the fundamental frequency and corresponding mode shapes. A qualitative assessment of stone masonry by means of masonry quality index (MQI) is also provided. In a second step, the experimental works include the out-of-plane quasi-static loading tests of the two reinforced stone masonry walls using an airbag to simulate the seismic loading.

Finally, a finite element model was prepared and calibrated with the experimental results. In addition, the paper presents a parametric study intended to evaluate the influence of the geometrical configuration of the reinforcements on the overall out-of-plane response of the stone masonry walls.

2. Testing specimens: geometry and construction process

The stone masonry walls analysed in the present work were designed taking into account the geometrical features commonly found in stone masonry walls from vernacular buildings in the northern region of Portugal [24]. In order to study the effect of the connections between frontal and transversal walls on the out-of-plane behaviour of frontal walls, masonry walls specimens with U-shaped plan configuration were adopted (Figure 1). The majority of vernacular buildings in northern Portugal are usually limited to one floor and the stone masonry walls are mostly double leaf. The span of the façades does not exceed 10 m, often ranging from 3.0 to 4.5 m. Therefore, specimen geometrical parameters were set according to the most common dimensions observed in the reference area (Northern Portugal). The wall specimens were finally established with a span of 4.50 m, with a height of 2.70 m and a thickness of 0.60 m. The slenderness ratio calculated is equal to 4.5. The same thickness (0.60 m) was assumed for the transversal walls, whose length was set at 2.0 m. Due to laboratory space restrictions, it was decided to test half scale reduced specimens (1:2), i.e. the dimensions of prototype wall were reduced to half, including the stones through the thickness, see Figure 1. The same criteria were applied to define the geometrical configuration of the unreinforced wall (Wall_Ref) [21].

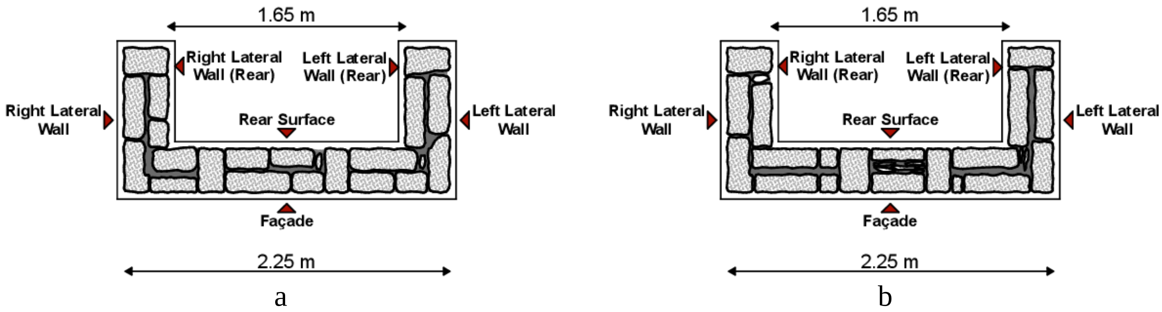

Figure 1 – Plan cross section of the tested specimens through the second masonry course: Wall_Stl (a) and Wall_Tmb (b)

Preprint version, Reference: Murano, A., Ortega, J., Vasconcelos, G., Rodrigues, H. Influence of traditional earthquake-resistant techniques on the out-of-plane behavior of stone masonry walls: experimental and numerical assessment. *Engineering Structures* (2020). https://doi.org/10.1016/j.engstruct.2019.109815

The walls were built by an experienced mason, who roughly followed a set of initial technical drawings indicating stone dimensions and the position of the headers (through stones). The masonry walls were built on top of a reinforced concrete beam base with a height of 0.20 m. Figure 2 depicts different stages of the construction related to Wall_Ref, Wall_Stl and Wall_Tmb. Parallelepiped granite stones with mostly regular configuration were used (Figure 2). Through-stones were also used to ensure an adequate connection between the wall leaves. Their use is widely common in vernacular architecture building practice to promote monolithic behaviour of the walls and thus improve its stability by attaining a more uniform stresses distribution through the cross section. Through-stones were distributed throughout the area of the walls, with a minimum of two per row. They were vertically misaligned to spread their beneficial coupling effect. In order to provide effective wall-to-wall connections, special attention was given to the construction of the corners, providing adequate interlocking between the stones of the transversal and frontal walls.

a b c

Figure 2 – Details of different construction stages: Wall_Ref [21] (a), Wall_Stl (b), Wall_Tmb (c)

A pre-mixed hydraulic lime mortar was used to lay the stone units and fill the vertical joints. Small stone pieces were also inserted to fill the voids between the stone units through the thickness. In order to assess the evolution of the compressive and flexural strength of mortar according to the guidelines provided in EN 1015-11 [25], 9 specimens were **cast** before the construction of the two walls. The flexural strength of the mortar was 3.15 N/mm^2, 3.21 N/mm^2 and 4.06 N/mm^2 after 7, 14 and 28 days respectively. The compressive strength of the mortar was 11.64 N/mm^2, 12.69 N/mm^2 and 14.29 N/mm^2 after 7, 14 and 28 days respectively, being thus higher than the expected strength at 28 days, namely 10 N/mm^2.

From a morphological point of view, it is possible to say that the tested specimens represent walls made of regular roughly cut stone units, aligned bed joints and not-aligned vertical head joints. The stone units length is between 0.30 and 0.50 m and the height is approximately 0.22 m. The thickness of the stones unit ranges from 0.10 m to 0.20 m, so that the two-leaf cross-section could be built. The voids among the stone units were filled with rubble stones and the same mortar used to lay the units (Figure 3).

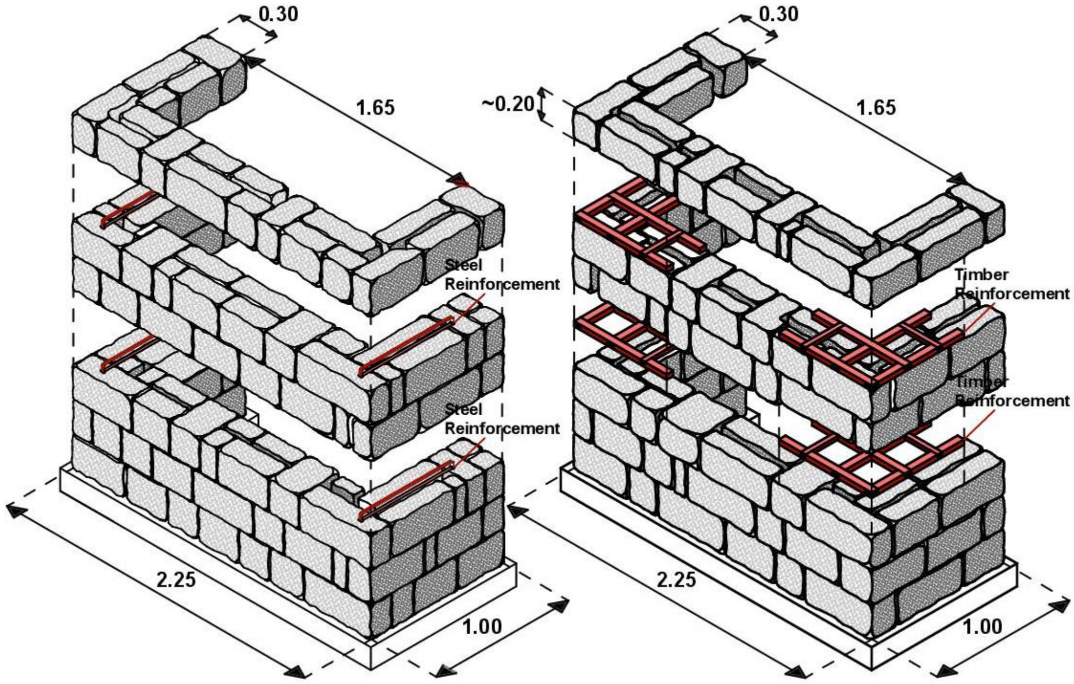

a b

Figure 3 – Axonometric view: Wall_Stl (a) and Wall_Tmb (b)

As previously mentioned, two types of earthquake resisting solutions aimed at improving the connection between transversal and frontal walls were adopted (Figure 3). The first earthquake resistant technique consists of steel bars installed in both wall corners at the 3rd and 5th masonry course (2 for each side). Steel reinforcing elements have a length equal to 0.70 m and a thickness equal to 4.50 mm. The edges of the steel ties (length equal to 45 mm) were bent downwards and inserted in pre-drilled holes in the stones. They allowed to effectively anchor the reinforcing elements to the masonry units.

The second earthquake resistant technique solution consists of timber-laced elements embedded within the corners of the wall in the same location selected for the steel braces, namely at the 3rd and 5th masonry courses. Each corner brace consists of two longitudinal timber elements parallel to the walls connected by transversal timber elements (Figure 3). The length of the longitudinal element is 0.70 m. The cross-section dimensions of the timber members were 50 x 35 mm^2 for the longitudinal elements and 35 x 25 mm^2 for the transversal elements. The connections among timber elements have a configuration similar to nailed half-lap joints. Due to the irregularity of the bed joints, the empty spaces formed between the timber elements and stone were filled with rubble stones and mortar. Some small incisions were chiselled on the smooth surfaces of the timber elements, in order to foster the adherence between mortar and timber. In order to prevent an increase of the height of the wall due to the addition of timber elements, the height the stones units placed at the 5th and 6th masonry courses were reduced.

Once the construction process of the walls was concluded, the density of the walls was estimated. The total density of the walls can be estimated starting from the values of density of the constituting materials, namely mortar and stone units. The density of mortar was measured as 1821 kg/m^3, whereas the average density of granite was assumed equal to 2600 kg/m^3 [26]. The procedure applied is based on an approximate calculation of stone and mortar area per square meter (Table 1). The volume of the materials was estimated from detailed drawings with the dimensions of the stone units taken during the construction of the walls.

Table 1 – Density assessment (Reference Surface = 1 m^2)

	Stone Units Av. Volume (m^3)	Mortar Average Volume (m^3)	Stone Units Av. Weight (kg)	Mortar Average Weight (kg)	Stone Units + Mortar Total Weight (kg)	Density (kg/m^3)
Wall 1	0.272	0.034	706	62	768	2513
Wall 2	0.251	0.045	652	81	743	2482

3. Assessment of stone masonry mechanical properties

The mechanical behaviour of traditional stone masonry highly depends on the quality of materials and on the masonry assemblage. Moreover, the mortar plays a significant role in assuring a good quality masonry bond. Non-destructive techniques (NDTs) allow obtaining quantitative and qualitative data of masonry walls, including the mechanical properties. NDTs are extremely useful to avoid using destructive testing when assessing historical constructions. Additionally, a preliminary evaluation of the masonry properties was carried out through the Masonry Quality Index method [27], simply based on the geometry of the walls. In summary the mechanical properties of the masonry were assessed by means of: (a) Masonry Quality Index (MQI) method; (a) Sonic tests, which are able to provide reference elastic mechanical properties that can be applied in numerical models; (b) Dynamic identification tests, which provide an estimation of the natural frequencies and mode shapes and can be used to calibrate the numerical models and to update, if necessary, the initially selected material properties.

3.1. Evaluation of Masonry Quality Index

A preliminary qualitative characterization of the masonry was carried out using the MQI method, which helps to estimate a possible range for the mechanical properties. This method consists of evaluating the presence (Fulfilled – F), the partial presence (Partially Fulfilled – PF) or the absence (Not Fulfilled – NF) of certain parameters which contribute to define the “rule of the art” for an “ideal” masonry wall. Once a MQI value for a loading condition is known, it is possible to compute mechanical parameters, such as compressive strength (f_m) and Young modulus (E), using specific correlation curves [27]. As an example, Figure 4 shows the graphical procedure followed to determine horizontal joints characteristics (HJ), vertical joints characteristics (VJ) and wall connection effectiveness (WC) in Wall_Stl. Table 2 and Table 3 present the outcomes resulted from the application of the MQI method according to the criteria and guidelines proposed by Borri et al. [27] [28].

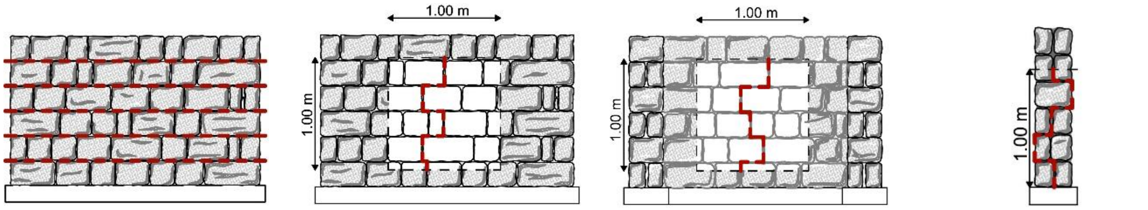

Figure 4 – Example of HJ, VJ and WC parameter definition and application to Wall_Stl

Table 2 – Masonry Quality Index for Wall_Ref, Wall_Stl and Wall_Tmb

	Masonry Quality Index Vertical Load (V) – $MQI_{,V}$							
	HJ	WC	SS	VJ	SD	MM	SM	$MQI_{,V}$
Wall_Ref	2	1	1.5	0.5	0.5	0.5	1	6
Wall_Stl	2	1	1.5	1	0.5	0.5	1	6.5
Wall_Tmb	2	1	1.5	1	0.5	0.5	1	6.5

Table 3 – MQI mechanical parameters for Wall_Ref, Wall_Stl and Wall_Tmb

	$MQI_{,V}$	Category	Compressive strength (N/mm^2)		Young modulus (N/mm^2)	
			$f_{m,MAX}$	$f_{m,MIN}$	E_{MAX}	E_{MIN}
Wall_Ref	6	A	5.60	3.60	**2189**	**1555**
Wall_Stl	6.5	A	6.15	3.99	**2375**	**1697**
Wall_Tmb	6.5	A	6.15	3.99	**2375**	**1697**

3.2. Sonic tests

Sonic testing is based on the elastic wave method and consists of measuring the velocity of the wave propagation within a certain volume under evaluation. Direct test aims to measure the velocity (V_P) of primary waves (P-waves), whereas indirect tests can be used to measure both the velocity of P and R-waves (V_R) [29]. These velocities are dependent on the physical properties of the analysed solid, such as density, Poisson's ratio and dynamic modulus. Therefore, this technique can provide significant outcomes not only regarding the quality of the masonry, but also on the prediction of elastic properties using the following expressions [29]:

$$\frac{V_P}{V_R} = \sqrt{\frac{2 \cdot (1-\nu) \cdot (1-\nu)^2}{(1-2\nu) \cdot (0.87 + 1.12\nu)^2}} \tag{1}$$

$$V_P = \sqrt{\frac{E}{\rho} \cdot \frac{(1-\nu)}{(1+\nu) \cdot (1-2\nu)}} \tag{2}$$

These expressions were developed for solid, elastic, isotropic and homogeneous materials. Therefore, they have to be used with extra care if applied to masonry, being aware that the results have to be interpreted as an approximate first estimation of the mechanical properties.

Preprint version, Reference: Murano, A., Ortega, J., Vasconcelos, G., Rodrigues, H. Influence of traditional earthquake-resistant techniques on the out-of-plane behavior of stone masonry walls: experimental and numerical assessment. *Engineering Structures* (2020). https://doi.org/10.1016/j.engstruct.2019.109815

Considering that the values of the compressive strength of the mortar used in the construction of the walls at 7 and 14 days were very close each other, the non-destructive tests were carried out 7 days after the construction of both walls. It was considered that this variation of the compressive strength of the mortar would not affect significantly the results obtained in sonic tests.

The equipment used included one instrumented impact hammer (PCB Model 086D05) with a measurement range of ±22240 Npk, one accelerometer (PCB model 352B) with a measurement range of ±5 g and 1000 mV/g sensitivity, a personal computer, cables and a data acquisition system from National Instruments. In direct sonic tests, the hammer and the accelerometer are aligned at opposite sides of the stone masonry wall. The wave propagation velocity is computed by measuring the time between the emission of the input signal by the hammer and its reception by the accelerometer, divided by the wall thickness. In indirect sonic tests, both the hammer and the accelerometer are placed in the same face of the wall in a vertical or horizontal line. The velocity can be computed, in this case, using the distance between the hammer and the accelerometer. Both P and R waves sonic velocities have been obtained throughout the elevation of the frontal wall. The grid points used for the direct sonic tests are shown in Figure 5.

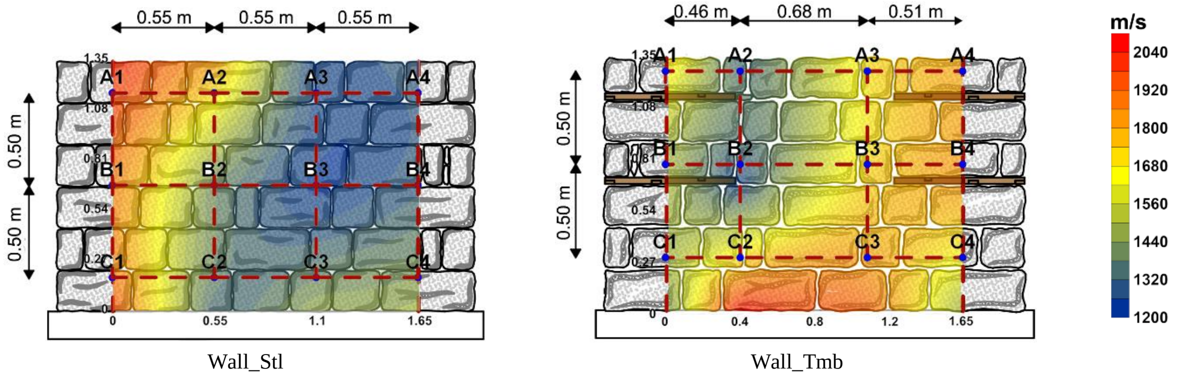

Figure 5 – Sonic test reference grid and P-waves velocity contour maps for both tested walls

Looking at the contour maps representing the distribution of velocities throughout the inspected surfaces of the masonry walls, it is possible to notice lower values related to the specimen Wall_Stl. The velocity measured is more homogenous in the wall reinforced with the timber laced beam (Figure 5). In order to analyze the reliability of the collected sonic data, some contour maps, representing the velocity distribution along the horizontal cross section of the analysed walls, are presented in Figure 6. The low P-waves velocity values characterizing Wall_Stl are probably due to the presence of voids affecting the overall quality of the masonry (Figure 6-a). The results related to Wall_Tmb highlight a more uniform pattern and higher velocity values but some variations are observed due to local construction flaws (Figure 6-b).

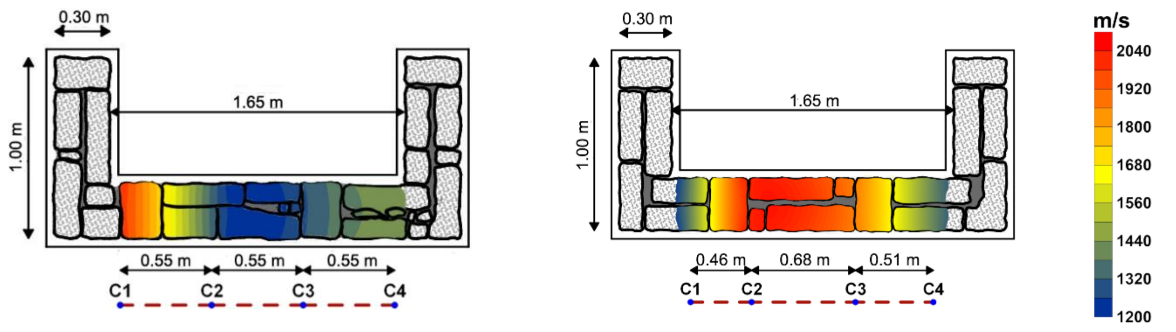

(a) (b)

Figure 6 –P-wave velocity distribution through horizontal cross-section: Wall_Stl (a) and Wall_Tmb (b)

The mean values of the velocities (V_P and V_R) obtained for each wall and the values estimated for the density shown in Table 1 were adopted for the prediction of the elastic material properties (E and ν). Table 4 shows the results of direct and indirect sonic tests in terms of mean values and standard deviation (STD) of velocities obtained for both tested specimens. The values related to the reference wall (Wall_Ref) are also reported [21]. The dynamic modulus obtained for Wall_Ref is higher than the ones obtained in specimens Wall_Stl and Wall_Tmb. As previously observed for the velocity distribution in the horizontal cross section of the experimental models (Figure 6), the presence of voids could affect the measurements. The values obtained for the Poisson's ratio for Wall_Stl and Wall_Tmb are within typical values obtained for this type of granite masonry walls, which usually range between 0.2 and 0.3 [26]. Moreover, the general low values of coefficient of variation, mainly for the direct tests, indicate that the results are consistent. The control of construction workmanship might have contributed to obtain this overall good construction quality of the walls.

Table 4 – Sonic test results

	Direct Sonic Tests V_P (m/s)			Indirect Sonic Tests V_P (m/s)			Indirect Sonic Tests V_R (m/s)			Poisson Ratio (ν)	Young Mod. E (MPa)
	Mean	STD	CoV (%)	Mean	STD	CoV (%)	Mean	STD	CoV (%)	Mean	Mean
Wall_Ref	1955	230	12	-	-	-	-	-	-	0.39	4115
Wall_Stl	1381	209	13	1233	100	8	627	56	9	0.28	2960
Wall_Tmb	1626	363	20	1270	77	6	693	40	6	0.25	3450

3.3. Dynamic characterization tests

Dynamic characterization tests allow to estimate the dynamic characteristics of a structure in terms of natural frequencies and vibration modes. Therefore, it is a fundamental tool for the calibration of numerical models. The dynamic characterization tests were carried out, in both specimens, before the out-of-plane test (undamaged condition) and after the out-of-plane test (damaged near-collapse condition). The results of the dynamic identification tests can also be used as a measure to correlate damage as this reflects a variation of the natural frequencies and stiffness reduction [30] [31].

The dynamic tests were carried out using uniaxial accelerometers placed in 12 different predefined points within different test setups for each wall. For each setup, a fifteen-minute reading was acquired using a sample frequency rate of 200 samples/s with ambient vibration. The sensor layout related to the tested prototypes is presented in Figure 7. One reference accelerometer (AC0) is common in all setups, as it can be seen in the red arrow shown in Figure 7-b. The remaining locations were chosen where higher displacements amplitudes were expected, in order to allow a proper definition of the mode shapes. Accelerations were measured in both directions at some locations in order to detect both possible in-plane and out-of-plane mode shapes. The equipment used included accelerometers (PCB model 393B12) with a measurement range of ±0.5 g and 10,000 mV/g, a personal computer, cables and a data acquisition system.

a b

Figure 7 – Sensor placed during one setup (a); Artemis software axonometric scheme of the sensors location (b)

The modal estimation was carried out by using ARTeMIS software, which allows analyzing the results from all test setups simultaneously. The mode shapes were drawn in ARTEMIS by means of linear interpolation, starting from data recorded in discrete sensors locations (Figure 7-b). The peak values of frequency were selected using Frequency Domain Decomposition (FDD) and Subspace Identification-Unweighted Principal Components (SSI-UPC) technique. The results of the analyses have been compared using the Modal Assurance Criterion. Figure 8 shows the first three identified mode shapes and natural frequencies for Wall_Ref [21], Wall_Stl and Wall_Tmb.

In all the tested prototypes, the first mode consists of the out-of-plane vibration of the façade, as expected. An out-of-plane movement of the lateral walls characterizes the second mode shape, being this trend mostly visible in Wall_Tmb, whereas the third mode presents a torsional shape. In both cases, the values of frequency resulted from the analysis are close to each other, which can be due to the similarities of the experimental models in terms of physical properties (mass and density) and geometrical configuration. On the other hand, the first natural frequency in Wall_Ref appears to be slightly higher if compared to Wall_Stl and Wall_Tmb.

Preprint version, Reference: Murano, A., Ortega, J., Vasconcelos, G., Rodrigues, H. Influence of traditional earthquake-resistant techniques on the out-of-plane behavior of stone masonry walls: experimental and numerical assessment. *Engineering Structures* (2020). https://doi.org/10.1016/j.engstruct.2019.109815

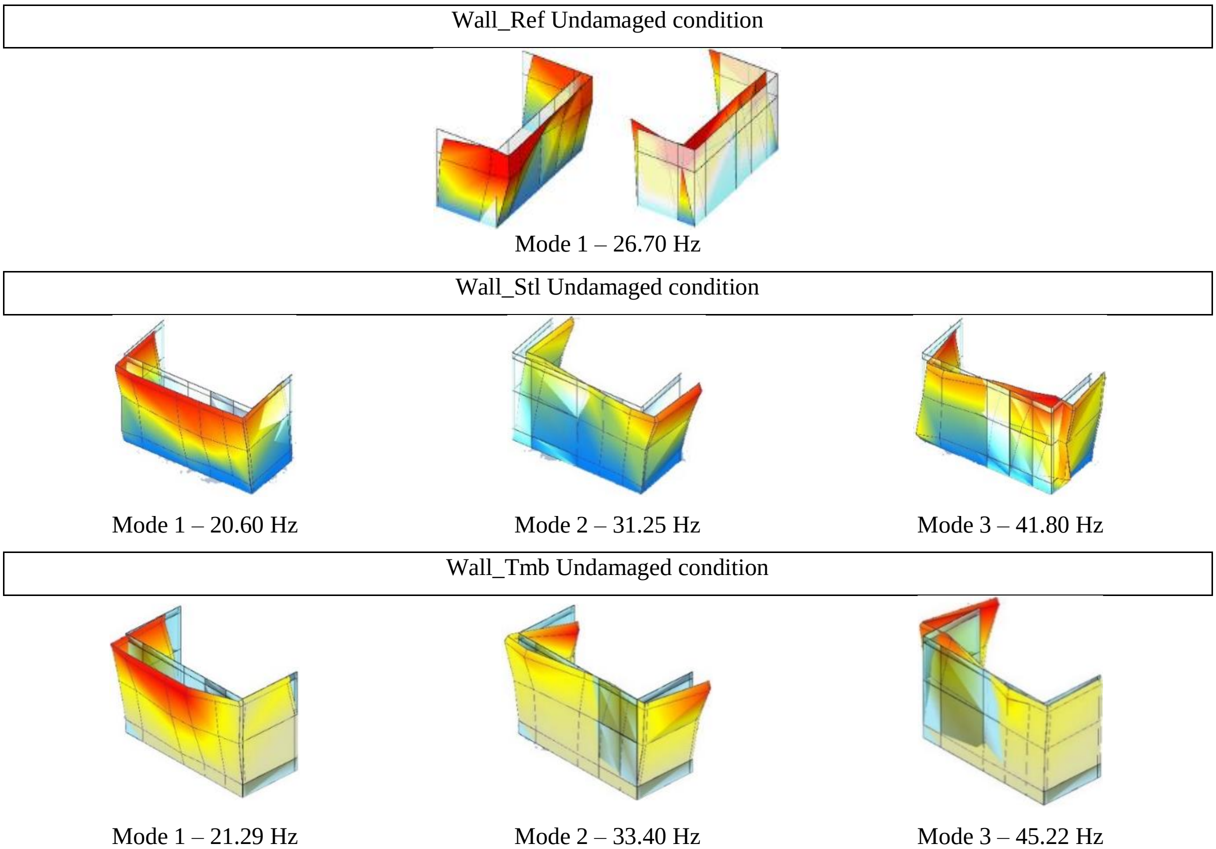

Figure 8 – Main mode shape and natural frequencies of Wall_Ref, Wall_Stl and Wall_Tmb

4. Assessment of out-of-plane experimental behaviour of reinforced stone masonry walls

This section describes the out-of-plane quasi-static loading tests carried out on the two reduced scale models (1:2). They were tested using an airbag to apply a distributed uniform load to the rear surface of the wall. The test setup is analysed in detail, as well as the main outcomes of the tests (e.g. cyclic response, displacements, crack pattern, and dissipated energy).

The performances of the reinforced prototypes (Wall_Stl and Wall_Tmb) are compared to the global response of Wall_Ref [21]. The main aim of the experimental campaign was the assessment of the contribution of the applied earthquake resistant techniques to enhance the out-of-plane performance of the stone masonry walls. It is important to point out that the overall testing setup and experimental procedures applied to Wall_Ref, Wall_Stl and Wall_Tmb are the same.

4.1. Test setup, procedure and instrumentation

The loading configuration used in the out-of-plane test involves an airbag with an area of 1.65x1.35 m^2 to apply a uniform horizontal load to the frontal wall that simulates the seismic action. Additionally, a vertical load was also applied to the transversal walls to simulate the self-weight of a timber roof (Figure 9). A supporting steel frame was placed between the reinforced concrete reaction wall of the laboratory and the airbag. Wooden planks were attached to the steel supporting structure in order to create a smooth contact surface where the airbag can be placed, avoiding any possible damages (Figure 9). Four load cells were placed between the steel profiles and the reaction wall at the level of the horizontal steel profiles. These cells allowed recording the load applied by the airbag to the wall, overcoming the issue related to the calculation of the contact area between the airbag and the prototype, which may vary throughout the test due to the deformation of the wall.

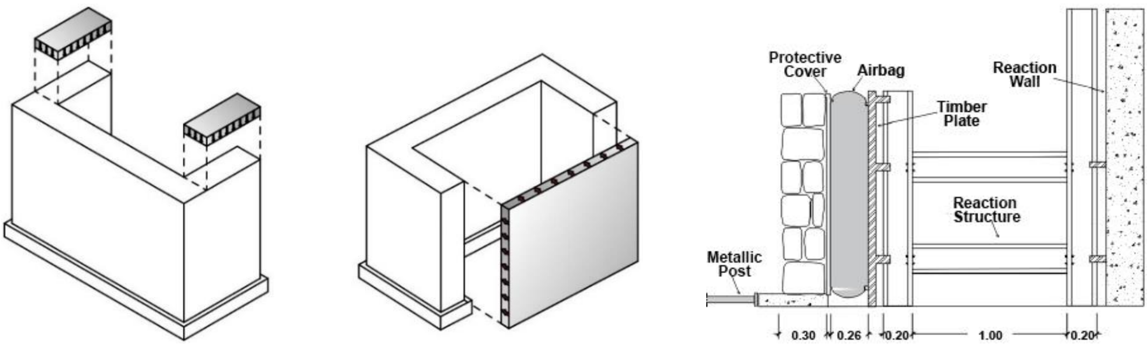

a b

Figure 9 – Load configuration (a) and test setup configuration (b) adopted for the out-of-plane test

At the top surface of the transversal walls, two steel profiles were placed in order to even the vertical load applied through two vertical hydraulic actuators. These actuators were placed between the steel profiles and the reaction slab, see Figure 10-a. A vertical load of 10 kN, corresponding to a normal compressive load of approximately 0.05 MPa, was applied in each transversal wall. Two steel posts were placed at the back of the transversal walls between the concrete base and the reaction slab to avoid

Preprint version, Reference: Murano, A., Ortega, J., Vasconcelos, G., Rodrigues, H. Influence of traditional earthquake-resistant techniques on the out-of-plane behavior of stone masonry walls: experimental and numerical assessment. *Engineering Structures* (2020). https://doi.org/10.1016/j.engstruct.2019.109815

a possible overturning of the concrete base (Figure 10-b). In order to avoid any possible sliding displacements, six steel posts were also placed between the concrete base of the prototype and the laboratory reaction wall (Figure 10-c).

a b c

Figure 10 – Details of out-of-plane testing setup: Hydraulic actuators (a); metallic posts placed to counteract uplift movements (b) and sliding movements (c)

The horizontal load was applied at the frontal wall after the stabilization of the vertical load. The out-of-plane test was carried out under displacement control, being the control point located at the top of the frontal wall at mid-span, where the highest displacement was expected. The procedure applied during the test consists of imposing positive incremental displacements repeated two times in order to detect possible stiffness and strength degradation after reaching the peak load. At the end of each series, an increment equal to 1.4 times the latest displacement is applied to define the new displacement threshold of the following cycle. The pressurization and depressurization of the airbag was carried out in a controlled way using LabView software based on the displacement-time history defined for the out-of-plane test (Figure 11-a). The airbag has two pressure valves, which allow to inflate the airbag until a certain level of pressure that is enough to attain the imposed lateral displacement (Figure 11-b). Once the control displacement is reached, the air in the airbag is released until zero displacement in the early stages of the out-of-plane testing. When the non-linear response of the wall is activated, the unloading is only possible up to a residual displacement associated to the permanent deformation of the wall.

Preprint version, Reference: Murano, A., Ortega, J., Vasconcelos, G., Rodrigues, H. Influence of traditional earthquake-resistant techniques on the out-of-plane behavior of stone masonry walls: experimental and numerical assessment. *Engineering Structures* (2020). https://doi.org/10.1016/j.engstruct.2019.109815

a b

Figure 11 – Displacement-time law history (a); airbag pressure system (b)

The monitoring of the displacements of the frontal wall during the out-of-plane test was carried out using linear variable differential transducers (LVDTs). Figure 12 shows the LVDTs setup in Wall_Stl and Wall_Tmb façade. Note that LVDTs are depicted using a blue dot and an identification number. Sixteen monitoring points were set in the façade of the steel reinforced wall (Wall_Stl), whereas 14 points were defined for Wall_Tmb. Moreover, 2 displacement transducers were placed in the transversal walls of the first reduced scale specimen (Wall_Stl), in order to measure possible cracking and detachment of the frontal walls with respect to the transversal walls. Due to the presence of timber reinforcement, 4 displacement transducers were placed on the transversal walls of the specimen Wall_Tmb. They were intended to assess the performance of the timber elements, trying to detect possible detachments at the interface between timber and stone/mortar.

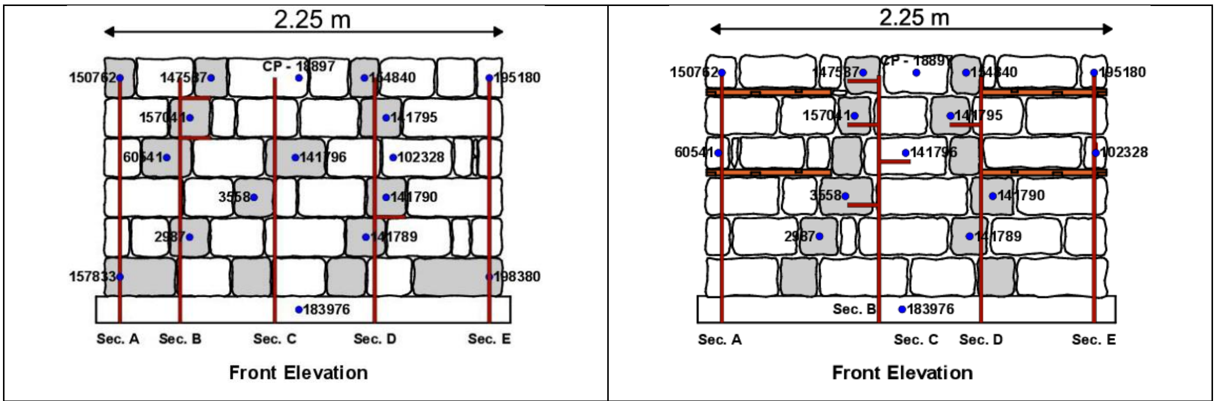

a	b

Figure 12 – Location of LVDTs at: Wall_Stl façade (a) and Wall_Tmb façade (b)

In both testing procedures, a LVDT was placed at the concrete base of the wall in order to detect any possible sliding phenomena. Two more LVDTs were placed at the lateral side of the concrete base (in a vertical configuration) to monitor the possible overturning, see left elevation at Figure 12. The criteria applied to define the LVDTs location were the following: (a) the displacement transducers were always placed at the stones and not at the mortar joints; (b) they were placed following as much as possible a vertical alignment (not always possible due to the irregularity of the masonry bond); (c) whenever possible, they were placed at the through-stones so that the global deformation of the wall could be measured (marked in grey in Figure 12); (d) displacement transducers were also placed in the corner stones in order to measure a possible detachment of the frontal walls from the transversal walls.

4.2. Analysis of the cyclic response

This section analyses the cyclic response of the walls by showing: (a) load-displacement diagrams obtained from the out-of-plane tests; (b) damage pattern, including the evolution of damage and the failure mechanisms observed; and (c) evaluation of the seismic performance of the walls, in terms of energy dissipation capacity and the damage limit states defined by Eurocode 8 [32].

4.2.1. Load-displacement diagrams

The load-displacement diagrams obtained from Wall_Ref, Wall_Stl and Wall_Tmb are presented in Figure 13. The force represents the sum of the values recorded by the four load cells. The displacement is representative of the control point in the top mid span of the wall (CP-18897, see Figure 12). It can be observed that the out-of-plane behaviour of both reinforced walls (Wall_Stl and Wall_Tmb) is similar. Their response is characterized by a linear elastic regime that lasts almost until peak load, which is close in both specimens The differences are more significant in the post peak cyclic response, in terms of permanent deformation. Nevertheless, they are characterized in both cases by a relatively smooth softening corresponding to the decrease of the force for increasing lateral displacements. In Wall_Stl (steel reinforced experimental model), there is a more abrupt descending branch just after peak load, but then the load almost stabilizes for increasing out-of-plane displacements. At the same time, the permanent deformations increase considerably after a displacement of 20 mm, which is due to the detachment of the upper area of the wall with progressive sliding along the horizontal crack developed almost at mid height. This is also responsible for the stabilization of the lateral resistance, as damage localize in the top region of the wall. The softening branch recorded in Wall_Tmb gradually decrease up to the maximum imposed displacement (Figure 13), meaning that the progression of damage is more spread in the wall.

With respect to the unreinforced wall (Wall_Ref), a reduction of the initial stiffness is observed at around 40 kN. After that point, the wall still reaches a maximum resisting load of 45.65 kN) but shows a notably higher rate of deformation. The post-peak branch highlights progressively decreasing loading levels, from the maximum force attained, reaching a stable trend for increasing lateral displacement until the end of the test, see Figure 13.

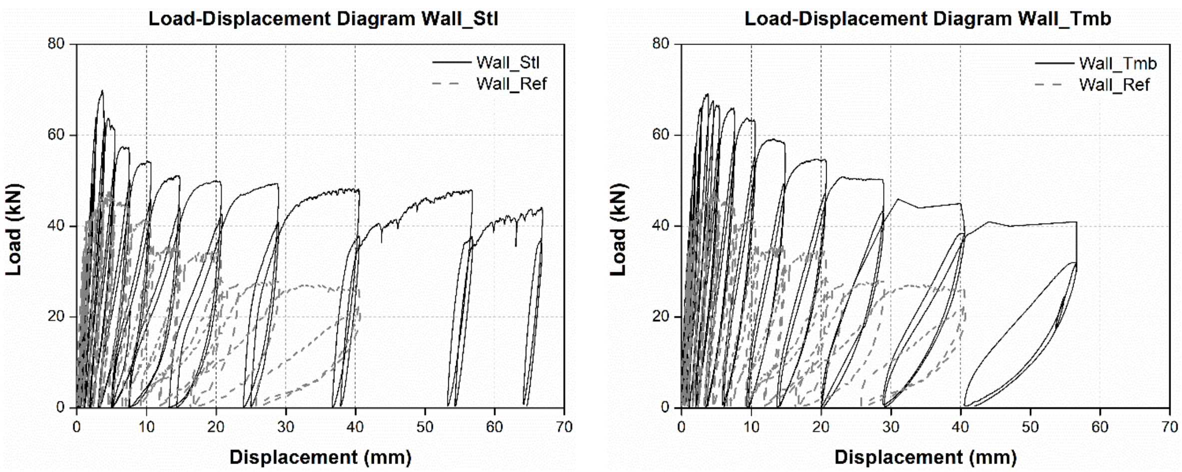

(a) (b)

Figure 13 – Load VS Displacement diagrams Wall_Stl (a) and Wall_Tmb (b)

The secant stiffness is calculated as the ratio between the maximum load and the maximum displacement in each step in the linear branch of the envelope curve. It is equal to 29.90 kN/mm, 23.15 kN/mm and 36.57 kN/mm in Wall_Ref, Wall_Stl and Wall_Tmb respectively. The most significant stiffness reduction occurs at 45.65 kN (Wall_Ref), at 61.32 kN (Wall_Stl) and 66.51 kN (Wall_Tmb). Even if both walls reach their maximum resisting load at around 70 kN, it is possible to notice a higher rate of deformation after the aforementioned stiffness decay thresholds (Figure 14-a). The maximum out-of-plane strength was 69.91 kN for the steel reinforced stone masonry wall and 68.91 kN for the timber reinforced stone masonry wall. Both techniques proved to be efficient enhancing the out–of–plane

Preprint version, Reference: Murano, A., Ortega, J., Vasconcelos, G., Rodrigues, H. Influence of traditional earthquake-resistant techniques on the out-of-plane behavior of stone masonry walls: experimental and numerical assessment. *Engineering Structures* (2020). https://doi.org/10.1016/j.engstruct.2019.109815

strength, leading in average to an increase of about 52% in the lateral resistance with respect to the reference wall. Figure 14-b presents a comparison among the monotonic envelop curves obtained for the three walls. The tests were stopped, for the sake of safety of the test setup, after reaching an out-of-plane displacement of approximately 67 mm (Wall_Stl) and 57 mm (Wall_Tmb). Moreover, the out-of-plane response was considered completely characterized for a strength degradation of about 60%.

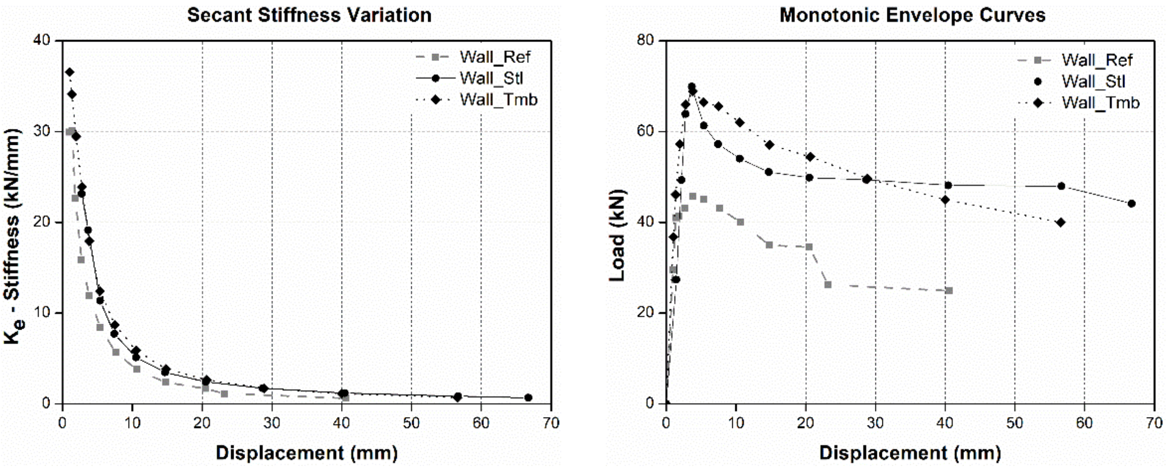

a b

Figure 14 – Analysis of the force-displacement diagrams: Secant stiffness variation (a); Monotonic envelope curves (b)

4.2.2. Cracking/damage patterns

The final damage patterns observed at the end of the out-of-plane tests for the reference wall (Wall_Ref) and reinforced walls (Wall_Stl and Wall_Tmb) can be seen in Figure 15. It should be noted that the cracking development at the rear surface of the frontal wall could not be followed due to the test setup configuration. Once the testing procedure finished and the airbag was removed, it was possible to record the final cracks at the back surface of the walls, see Figure 15.

In both reinforced walls, the cracks developed in an almost symmetric way. The damage pattern developed in Wall_Stl is characterized by diagonal cracks extending from the top to the bottom of the front elevation. Moreover, a considerable horizontal crack occurred along the top of the 4^{th} bed joint from the bottom base. The wall section delimited by the aforementioned cracks, consisting of the stone units laying on the central part of the 4th and 5th course from the bottom base, experienced some sliding displacements combined with rotation movements with respect to the right side. This phenomenon can be considered a sort of local mechanism mainly due to the inhomogeneity of the stone masonry bond, which rules the permanent deformation measured by the control LVDT, according to what was already mentioned in the previous section regarding the post-peak permanent deformations.

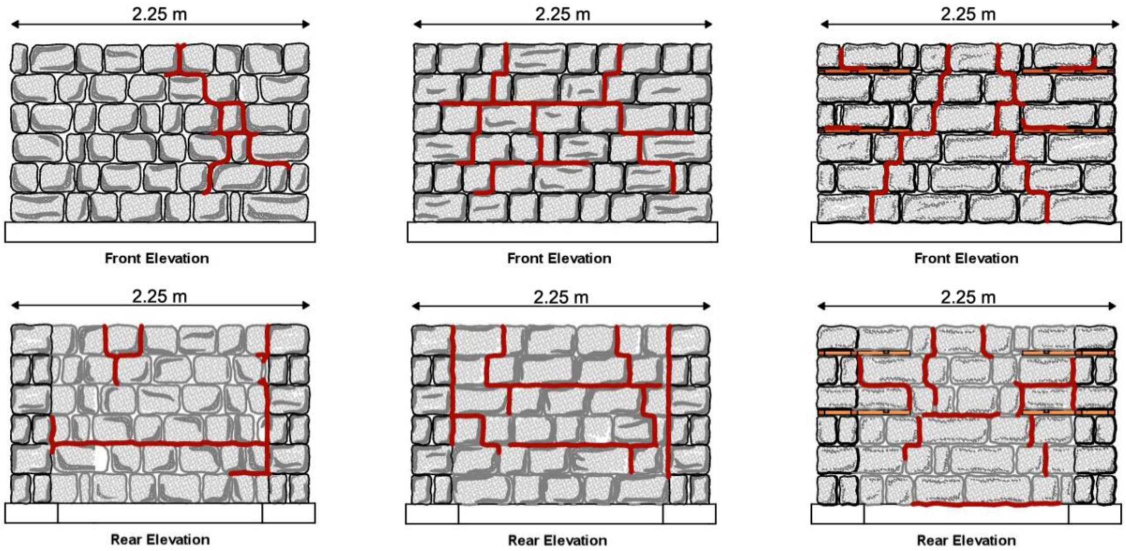

Wall_Ref Crack Pattern | Wall_Stl Crack Pattern | Wall_Tmb Crack Pattern

Figure 15 – Crack patterns (Wall_Ref, Wall_Stl and Wall_Tmb)

The damage pattern of wall Wall_Tmb shows more symmetric diagonal cracks in the front elevation. Timber reinforcements appeared to improve the overall behaviour of the wall, showing more uniform displacement field when compared to the displacement field recorded in the steel reinforced experimental model. In the specimen Wall_Ref, despite the arching mechanism developed, the out-of-plane resistance was controlled by the detachment of the frontal wall from the transversal walls according to what is shown in Figure 15.

The quality of masonry can, to a certain extent, explain the differences found in both reinforced specimens. Figure 16 correlates sonic test velocity maps with the crack pattern in Wall_Stl and Wall_Tmb. It is seen that the biggest cracks seem to primarily occur where low velocities were detected and, consequently, where lower quality of the masonry is expected.

The different crack and deformation patterns observed between both reinforced walls is clearly visible looking at the vertical and horizontal displacement profiles of the sections where the highest displacements were recorded (Figure 17). The behaviour of specimen Wall_Stl is characterized by peak displacements localized in the area corresponding to the large portion of masonry experiencing sliding and rotation movements. On the other hand, the displacements profile in timber reinforced wall appears less scattered, outlining a more gradual transition from the zero-displacement to the maximum-displacement points.

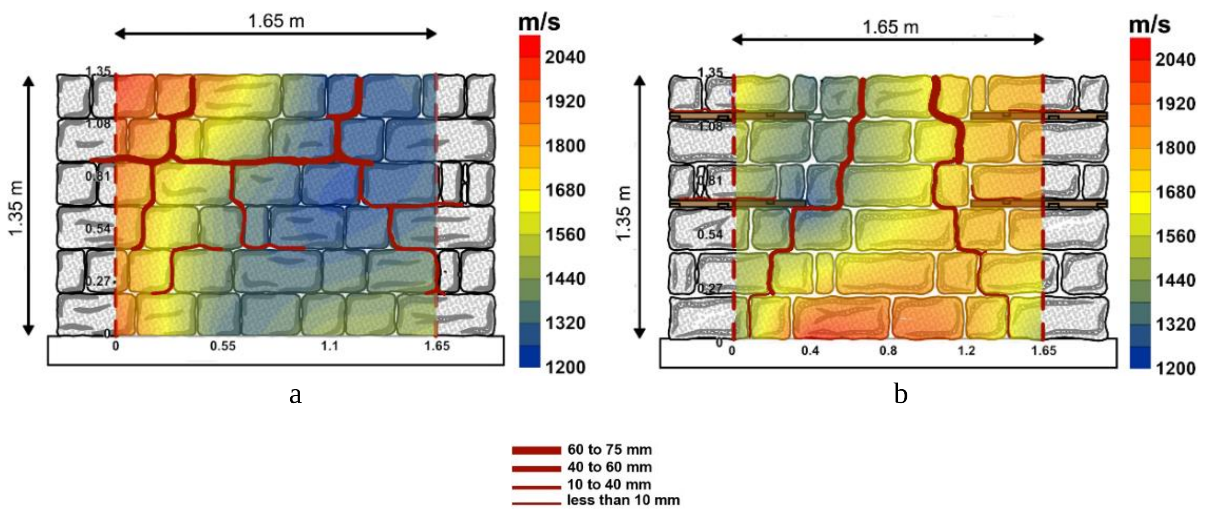

Figure 16 - Sonic test velocities distribution and crack patterns: Wall_Stl (a) and Wall_Tmb (b)

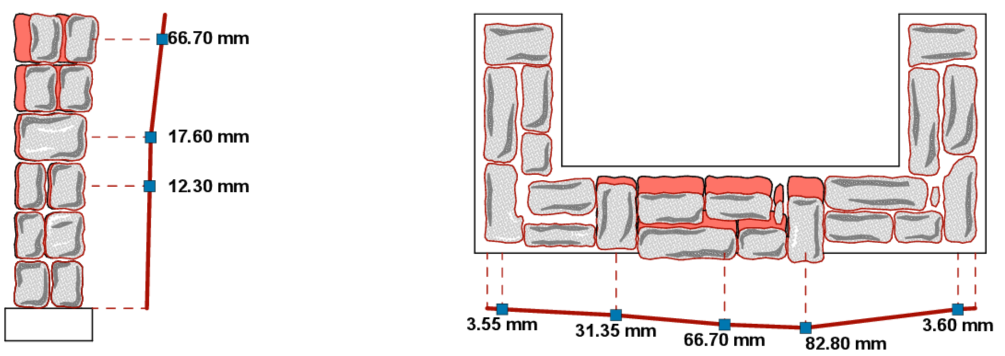

Wall_Stl – Section

Wall_Stl – 6th Masonry Course

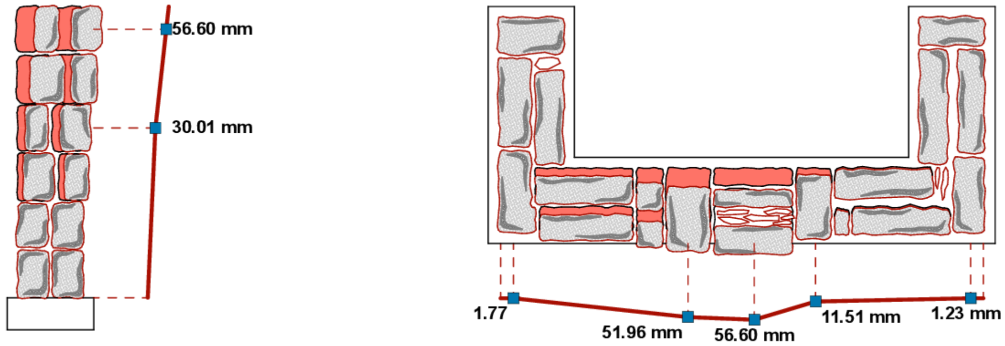

Wall_Tmb – Section   Wall_Tmb – 6th Masonry Course

Figure 17 – Wall_Stl and Wall_Tmb vertical and horizontal displacement profiles

Stepped cracks arising at the connection between front and transversal walls were visible in both walls. The stepped cracks in the frontal wall reinforced with timber laced reinforcement (Wall_Tmb) follow a preferential path outside the area where the timber elements were located. Vertical cracks also occurred along the inner corners in specimen Wall_Stl, visible from the rear façade. This pattern is not visible in specimen Wall_Tmb, which is attributed to the enhanced connection provided by the timber laced reinforcement.

Figure 18 and Figure 19 present the crack development throughout the test in the front elevation of Wall_Stl and Wall_Tmb respectively. Each crack pattern is drawn over the displacement fields obtained from the mesh of LVDTs located in the wall (see Figure 12). The contour maps were obtained through the measurements of all displacements at the frontal wall assuming a linear interpolation. The progress of damage is also associated to a point of the monotonic force vs displacement curve for reference.

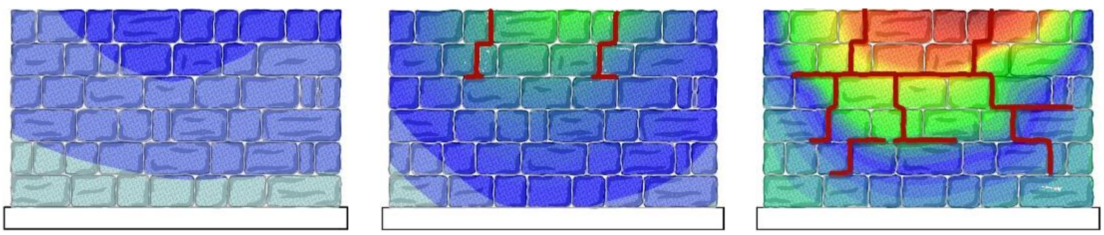

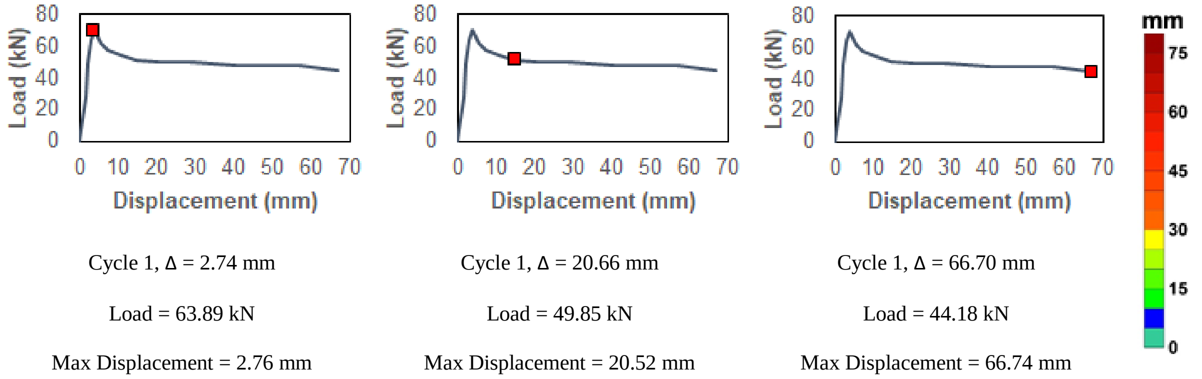

Figure 18 – Out-of-plane damage evolution in test Wall_Stl

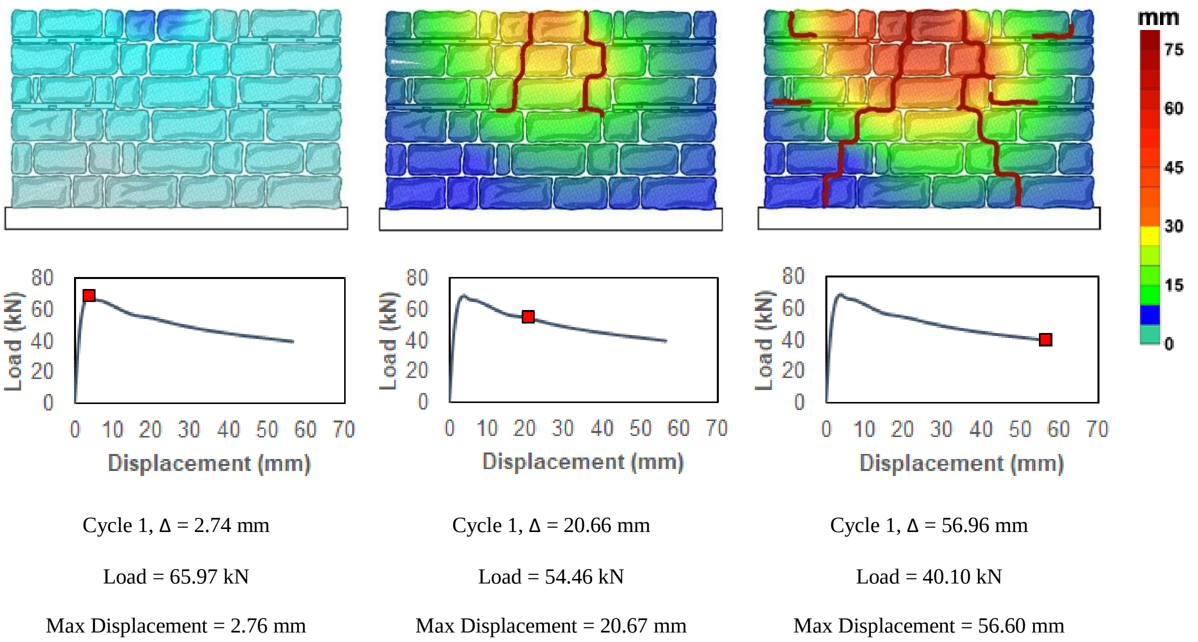

Figure 19 – Out-of-plane damage evolution in Wall_Tmb

It is observed that at the end of the linear regime, no significant cracks can be identified at the external surface of the frontal walls. The displacement fields obtained on both specimens suggest that both behave as a masonry panels restrained both at vertical borders and at bottom, which is particularly evident at the end of the out–of–plane test. This means that the connection of the frontal wall to the transversal walls, enhanced by the presence of embedded reinforcing elements, is effective and enables the development of the resisting arching mechanism. Nevertheless, this resisting mechanism is more evident in Wall_Tmb. The efficiency of the steel and timber elements on enhancing the connection of

Preprint version, Reference: Murano, A., Ortega, J., Vasconcelos, G., Rodrigues, H. Influence of traditional earthquake-resistant techniques on the out-of-plane behavior of stone masonry walls: experimental and numerical assessment. *Engineering Structures* (2020). https://doi.org/10.1016/j.engstruct.2019.109815

the frontal walls to the transversal walls is the main responsible for the increase of the out-of-plane resistance.

The final damage state of the walls was also assessed based on the variation of the frequencies and modes shapes obtained after the out-of-plane testing. With respect to the dynamic tests performed after the out-of-plane test, the first natural frequency experienced a reduction of 19.42% and 9.4% in Wall_Stl and Wall_Tmb, respectively. In the damaged condition, Wall_Ref presents a reduction of about 12.5% on the first natural frequency when compared to the undamaged condition (Figure 20).

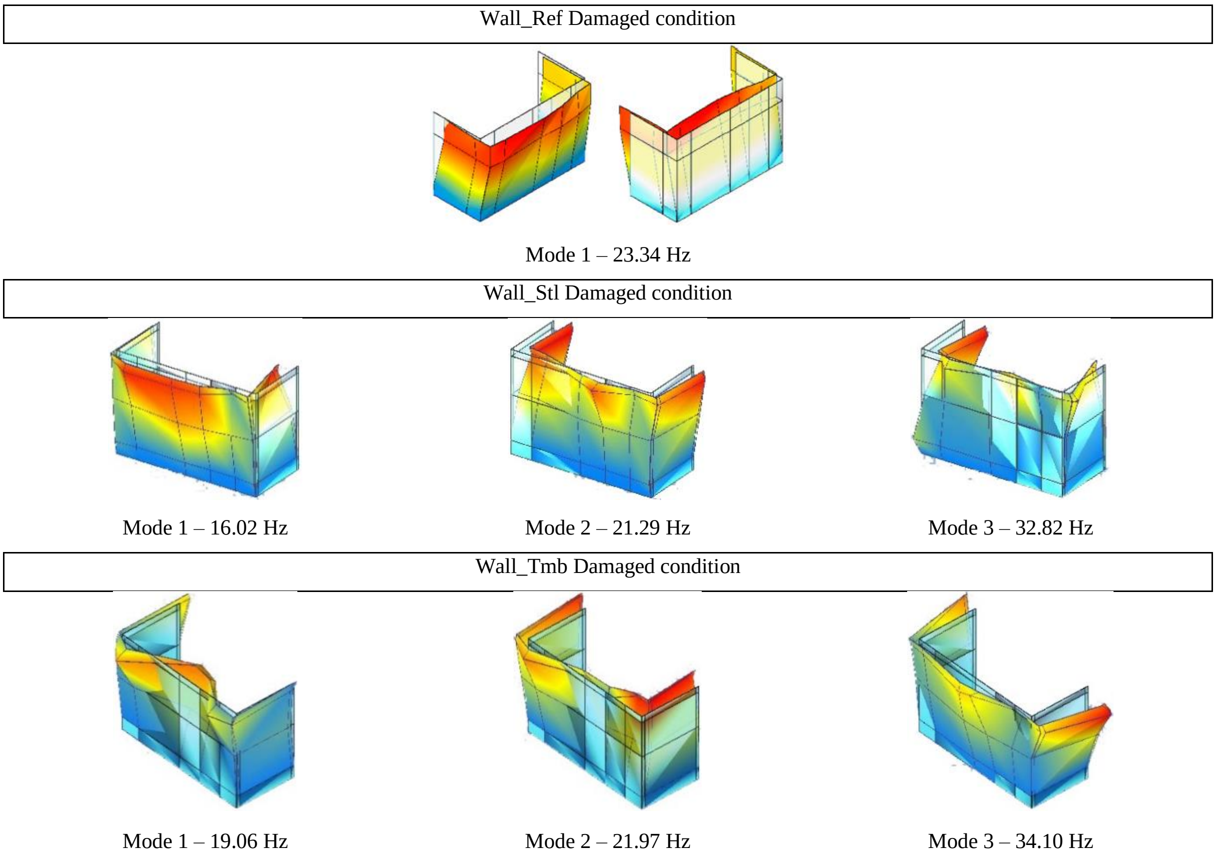

Figure 20 – Main mode shape and natural frequencies (damaged condition) in walls Wall_Ref, Wall_Stl and Wall_Tmb

The mode shapes related to the damaged conditions are clearly affected by the crack distribution occurred after the out-of-plane test. The first mode in Wall_Ref appears to maintain its original shape.

Preprint version, Reference: Murano, A., Ortega, J., Vasconcelos, G., Rodrigues, H. Influence of traditional earthquake-resistant techniques on the out-of-plane behavior of stone masonry walls: experimental and numerical assessment. *Engineering Structures* (2020). https://doi.org/10.1016/j.engstruct.2019.109815

The out-of-plane displacement is more significant in the left portion of the façade, but it gradually decrease reaching the section of the wall where an extended crack occurred (Figure 20).

Similarly, both in specimens Wall_Stl and in Wall_Tmb, the out-of-plane displacement is mainly concentrated in those parts of the façade delimited by the biggest cracks. In Wall_Stl, top and bottom corners show negligible displacement levels, whereas a considerable out-of-plane displacement characterizes the portion of façade, which experienced sliding phenomena during the airbag test. On the other hand, Wall_Tmb crack pattern ideally divides the façade into three sections according to the cracks observed, resulting in a phased out-of-plane displacement of the central portion of the front wall delimited by the timber-laced elements with respect to its corners.

4.2.3. Evaluation of seismic performance

The positive influence of the two techniques in the out-of-plane response of stone masonry walls is further confirmed by the evolution of the hysteretic energy dissipated during the test (Figure 21a). Dissipated energy is represented by the area enclosed by hysteretic loops obtained from load-displacement response records in the reference LVDT (control point). It is seen that for the same drift demand, the energy dissipated by Wall_Stl and Wall_Tmb is significantly higher when compared with unreinforced masonry wall (Wall_Ref). Looking at a drift level corresponding to 3%, the dissipated energy in Wall_Ref is 1998 kNmm, whereas for the same drift level the dissipated energy is 2882 kNmm (44% increase) and 3068 kNmm (53% increase) in Wall_Stl and Wall_Tmb, respectively.

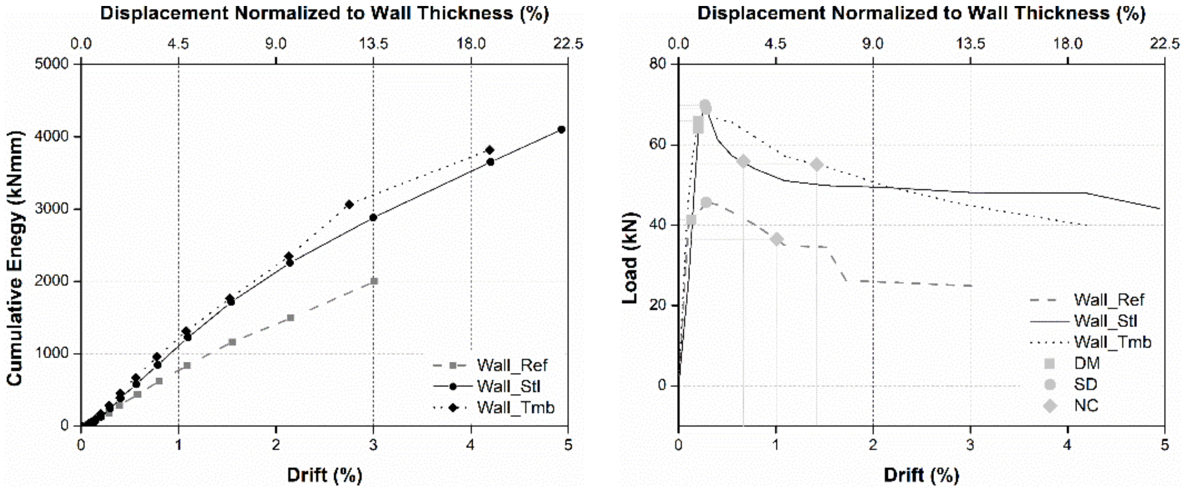

(a) (b)

Figure 21 – Energy dissipation capacity in Wall_Ref, Wall_Stl and Wall_Tmb (a); Limit states identification in Wall_Ref, Wall_Stl and Wall_Tmb (b)

Figure 21b provides information about the load and displacement corresponding to three damage levels or limit states defined by Eurocode 8 [32]. Following this approach and based on previous data of experimental campaigns on masonry buildings [33] [34], the different damage limit states were defined for the two walls: (1) Damage Limitation state (DM), which is associated to the point where a change of stiffness could be detected (H_{cr}, d_{cr}); (2) Severe Damage (SD) limit state, which is associated with the drift corresponding to the maximum out-of-plane strength (H_{max}, d_{Hmax}); and (3) Near collapse limit state (NC), which is associated to the lateral drift corresponding to a 20% decrease of the out-of-plane strength (H_u, d_{Hu}).

The walls present a very stiff initial behaviour, leading to very low values of lateral drift corresponding to the crack initiation (DM limit state). Due to the reduced nonlinearity before the peak load, relatively low values of lateral drift corresponding to severe damage limit states (SD) are also observed. The lateral drift corresponding to the NC damage limit state ranges between 0.66% and 1.42% for the steel reinforced and timber laced reinforced wall, respectively, whereas in the reference wall (Wall_Ref), the lateral drift related to NC damage limit state is equal to 1.01%. The first test (Wall_Stl) was stopped before the collapse, when the walls presented a lateral drift of approximately 5%, whereas the second test (Wall_Tmb) stopped when a lateral drift of 4.19% was reached. Even though the aforementioned limit states may be considered too conservative if applied to masonry walls under out-of-plane loading, it is possible to observe that the overall behaviour of the reinforced prototypes improved the performance of the walls in terms of the limit state corresponding to damage limitation (DM). The corresponding lateral drift increases from 0.13% (Wall_Ref) to 0.2% to reinforced walls (Table 5). The near collapse limit state (NC) is also attained for a higher lateral drift in case of Wall_Tmb. The lower lateral drift found for specimen Wall_Stl can be justified by the more sudden reduction of the lateral resistance after the peak load. In both reinforced walls, the performance levels are clearly attained for higher values of lateral resistance when compared to the reference wall.

Table 5 – Lateral drift and corresponding limit states

Reduced Scale Model	Damage Limitation (DM)		Severe Damage (SD)		Near Collapse (NC)	
	H_{cr} (kN)	d_{cr} (%)	H_{max} (kN)	d_{max} (%)	H_u (kN)	d_u (%)
Wall_Ref	41.42	0.13	45.65	0.28	36.52	1.01
Wall_Stl	63.89	0.20	69.92	0.27	55.94	0.66
Wall_Tmb	65.98	0.20	68.92	0.28	55.13	1.42

5. Numerical simulation

This section presents a methodology aimed at the preparation of a numerical model, calibrated with the experimental results collected from the dynamic tests and the out-of-plane tests performed on the walls. Subsequently, a pushover analysis reproducing the out-of-plane test is carried out, in order to compare the numerical and experimental results. Further discussion is included on the main differences in terms of crack pattern and load capacity of reinforced and unreinforced prototypes according to the numerical results. Finally, a parametric study mainly addressing the influence of geometrical configuration and number of reinforcing elements on the overall out-of-plane response is presented.

5.1. Finite element model

The numerical model of the wall was defined with DIANA software [35] using twenty-node tetrahedron solid 3D elements (CHX60). Since the model is intended to simulate the experimental test, the concrete base was also included in the numerical model using the same solid 3D elements. Plane quadrilateral interface elements (CQ48I) in a three-dimensional configuration were applied in order to reproduce the connection between the concrete base and the strong floor of the laboratory. Full connection was considered between the wall and the concrete base. Steel and timber reinforcing elements were modelled using tetrahedron solid 3D elements (CHX60). The steel and timber elements embedded within the wall were considered to be perfectly connected with the wall. Thus, common nodes share all degrees of freedom and no interface elements were used.

Both concrete, steel and timber elements have been analysed assuming a linear elastic behaviour. Linear elastic behaviour was considered also for the concrete base and a modulus of elasticity of 31 GPa and a Poisson's ratio of 0.2 were assumed. The Young modulus for steel was assumed equal to 210 GPa, whereas 7800 kg/m^3 and 0.3 were the values selected for density and Poisson ratio respectively. The Young modulus for timber was assumed equal to 10 GPa. The timber density and Poisson ratio were adopted as equal to 600 kg/m^3 and 0.2 respectively. The dimensions of the cross-section of the reinforced elements have been already presented in Section 2.

Figure 22 shows the final reference models for the three experimental models. In order to have a good representation of the strain and stress distribution, the overall size of the finite elements mesh is equal to 0.10 m. The mesh size adopted for the reinforcing elements was lower according to their geometrical characteristics. In the steel reinforcements, the mesh has been generated so that at least three finite elements defined the thickness of the solid. The mesh size in the timber elements is equal to 0.05 m.

Preprint version, Reference: Murano, A., Ortega, J., Vasconcelos, G., Rodrigues, H. Influence of traditional earthquake-resistant techniques on the out-of-plane behavior of stone masonry walls: experimental and numerical assessment. *Engineering Structures* (2020). https://doi.org/10.1016/j.engstruct.2019.109815

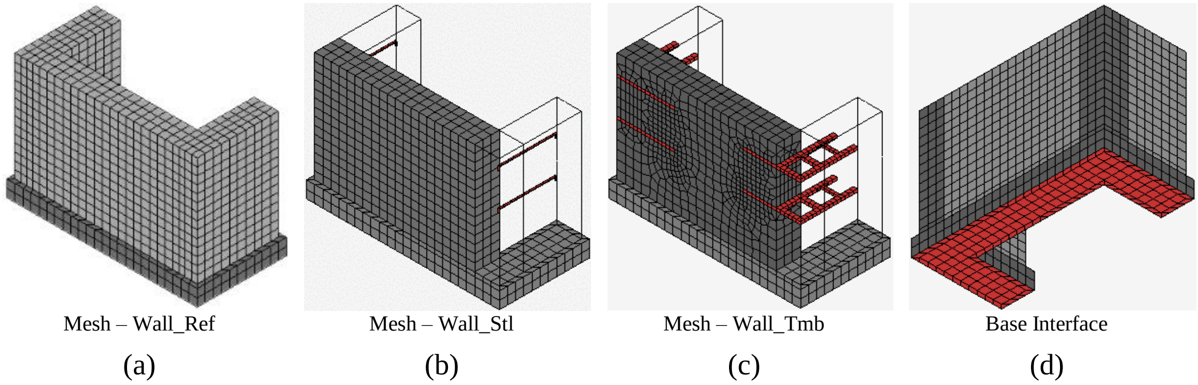

Figure 22 – Detailing on the finite element mesh: Reference model Wall 0 (a) Wall 1(b) and Wall 2 (c); interface elements used at the reinforced concrete base (d)

The material model adopted to represent the non-linear behaviour of the stone masonry is a standard isotropic Total Strain Rotating Crack Model (TSRM). The model describes the tensile and compressive behaviour of the material with one stress-strain relationship and assumes that the crack direction rotates with the principal strain axes. It is selected because of its robustness and simplicity, and because it has been proved to be very well suited for analyses predominantly governed by cracking or crushing of the material [36] [37]. An exponential softening function simulates the non-linear behaviour of the material in tension, whereas a parabolic function was adopted to describe the crushing behaviour in compression.

5.2. Calibration of the numerical model

The calibration process followed three steps based on the previously tests performed: (1) the elastic properties of the masonry were initially estimated based on the results of the sonic tests (Table 4); (2) a numerical modal analysis was performed and the frequencies and modes shapes obtained were compared with those obtained from the dynamic identification tests. This data enables to update the previous adopted elastic properties; and (3) finally, the force-displacement diagrams obtained in the out-of-plane tests allowed to define the nonlinear material properties. In this phase, the numerical force-displacement curves resulting from nonlinear static (pushover) were compared with experimental monotonic envelop of the reference wall.

It should be noted that in the second step of the calibration process, the stiffness properties of the interface elements placed at the base of the concrete beam to simulate the boundary conditions had to be also calibrated. The adjustment of the interface elastic properties was based on the displacement measured at the base of the concrete beam with the LVDT placed at the left external corner of the façade in Wall_Stl (see Figure 12) and at the mid-span of the concrete base of Wall_Tmb. For the unreinforced masonry specimen (Wall_Ref), the tangential stiffness in x and y direction was equal to 397 X 10^6 N/m^3 and the stiffness in the normal direction was equal to 992 X 10^6 N/m^3 [21]. For the speciemn Wall_Stl, an interface tangential stiffness of 247 X 10^6 N/m^3 was obtained for the horizontal x and y direction. The stiffness in the normal direction was set at 617.5 X 10^6 N/m^3. Regarding the specimen Wall_Tmb, an interface tangential stiffness of 257 X 10^6 N/m^3 was obtained for the horizontal x and y direction, whereas the stiffness in the normal direction was set at 640 X 10^6 N/m^3.

After this preliminary adjustment, the modal analysis was performed and the values of the natural frequencies were used to update the values of elastic modulus to consider in the nonlinear analysis. Table 6 shows the comparison between the numerical and the experimental results. The fitting of the numerical and experimental stiffness and lateral resistance led to reduce the experimental value of the Young modulus, see Table 6. The final values of the frequencies and mode shapes of the calibrated numerical modes by using the updated elastic properties, see Table 6, are 20.27 Hz and 21.01 Hz for the first mode in specimens Wall_Stl and Wall_Tmb, respectively. The modal participation in the out-of-plane direction is 75.55% and 75.85%. Furthermore, the first mode frequency of the reference wall (Wall_Ref) obtained was equal to 25.85 Hz, with a modal participation in the out-of-plane direction of 74.68%. The frequencies obtained for the unreinforced wall are slightly higher than the reinforced wall, but the mode shapes are the same. The validation of the frequencies was assessed based on the Modal Assurance Criterion (MAC). In comparison with the experimental values, the calibrated numerical models of the specimens Wall_Stl and Wall_Tm presented a very low error for the first mode (<2%). Average MAC values of 0.98 for the first mode and 0.91 for the second mode were obtained for specimen Wall_Stl. MAC values of about 0.84 (first mode) and 0.86 (second mode) were obtained for specimen Wall_Tmb. The slight asymmetry obtained in the experimental mode shapes due to the morphology of the masonry is not captured numerically, since the wall is simulated with a homogeneous material. This also leads to some differences in the numerical frequencies between Wall_Stl and Wall_Tmb. Nevertheless, the obtained MAC values show good agreement between numerical and experimental modes.

Table 6 – Experimental vs numerical mode shapes and frequencies (Wall_Ref, Wall_Stl and Wall_Tmb)

Experimental results					
Wall_Ref		Wall_Stl		Wall_Tmb	
Mode 1	Mode 2	Mode 1	Mode 2	Mode 1	Mode 2
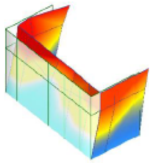	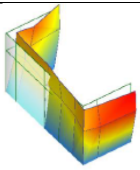	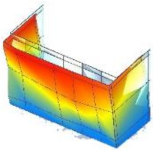	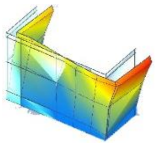	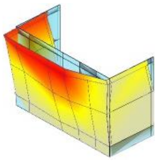	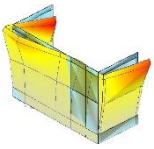
26.70 Hz	34.85 Hz	20.60 Hz	31.25 Hz	21.29 Hz	33.40 Hz
Numerical results					
Wall_Ref		Wall_Stl		Wall_Tmb	
Mode 1	Mode 2	Mode 1	Mode 2	Mode 1	Mode 2
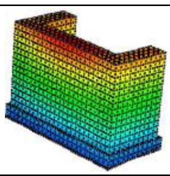	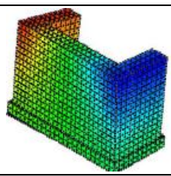	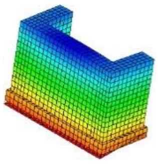	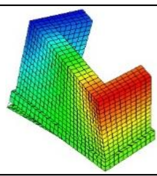	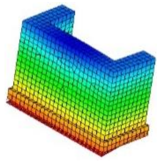	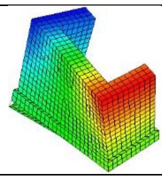
25.85 Hz	30.87 Hz	20.27 Hz	25.15 Hz	21.01 Hz	26.30 Hz
Error (%)					
3.10	11.40	2	24	1	27
MAC					
0.94	0.80	0.98	0.91	0.84	0.86

Table 7 – Linear and non-linear material properties after calibration procedure(after calibration)

	Linear Material Properties (Sonic tests)			Material properties (after calibration)				
	E (MPa)	ν	ρ (kg/m$^{3)}$	E_{up} (Mpa)	fc (MPa)	Gfc (N/m)	ft (MPa)	Gf1 (N/m)
Wall_Ref	4115	0.39	2495	3600	3.60	5760	0.07	12

Wall_Stl	2960	0.28	2513	2450	2.45	3917	0.07	12
Wall_Tmb	3450	0.25	2482	2974	2.97	4760	0.07	12

After the calibration through the modal analysis, pushover analyses were carried out to analyse the pre- and post-peak response of the numerical models. These analyses were primarily aimed to adjust the lateral resistance of the numerical model. The compressive strength was calculated following the suggestion of Tomaževič [8], in which the compressive strength can be obtained from the elastic modulus: $E=\alpha f_c$, where α ranges from 200 to 1000. The value of 1000 was assumed for this work. The tensile strength (f_t) was initially defined as 10% of the compressive strength, but it need to be further reduced up to 2% for Wall_Ref to fit the out-of-plane resistance of the reference model. This reduction resulted in a tensile strength value of 73300 N/m^2 (0.07 MPa), which was kept constant for Wall_Stl and Wall_Tmb. The compressive fracture energy was calculated by multiplying the compressive strength by a ductility index of 1.6 mm, according to recommendations of Lourenço (2009) [23]. The mode I fracture energy was considered as 12 N/m [23].

It should be stressed that the elastic properties resulting from the calibration process were updated from the values obtained in the sonic tests in the three different specimens. The tensile strength and fracture energy were taken equal in the three models, pointing out the relevance of these properties for the out-of-plane resistance of the stone masonry walls. This enabled also to assess the effectiveness of the reinforcing elements, at it will be analysed in the next section.

5.3. Numerical vs experimental results

This section shows the results of the nonlinear analysis performed with the updated material properties and assess the behaviour of the numerical models under out-of-plane loading. In these analyses, it should be noted that the same boundary and loading conditions adopted in the experimental tests were assumed. The vertical actions intend to simulate the self-weight of the roof structure and were uniformly distributed on the transversal walls. The out-of-plane action exerted by the airbag was simulated as a uniform distributed horizontal load applied in the rear surface of the frontal wall. The pushover analysis is based on the incremental application of the aforementioned horizontal load until collapse. The response of the structure is described by the capacity or pushover curve, which represents the horizontal load versus the displacement at the control point, which was taken at the same position where the control LVDT was placed in the experimental test (top mid-span of the frontal wall). Thus, the pushover curve can be directly compared with the force-displacement envelope obtained experimentally, see Figure 23.

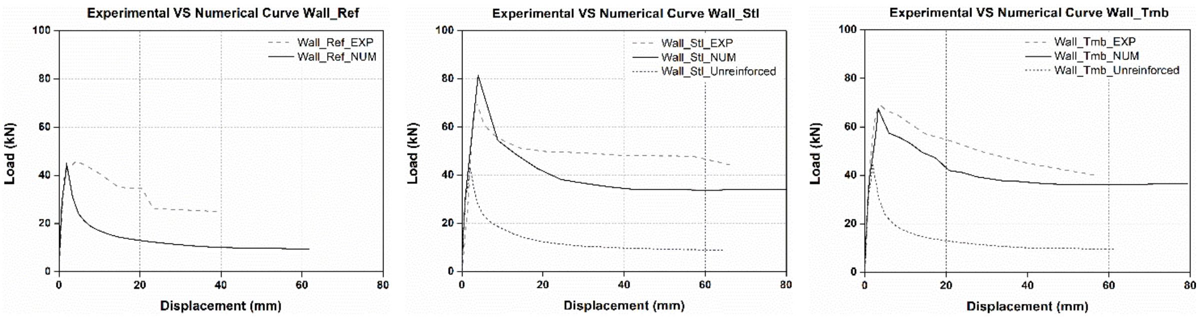

(a) (b) (c)

Figure 23 – Experimental vs Numerical capacity curve: Wall_Ref (a), Wall_Stl (b), Wall_Tmb (c)

From the results obtained, it is possible to observe that the pre-peak behaviour of three stone masonry walls is accurately simulated, but the numerical post-peak branch in Wall_Ref differs considerably from the experimental monotonic envelop. Similarly, the experimental behaviour observed in specimen Wall_Stl was characterized by a local mechanism involving a significant sliding of a portion of the front wall, resulting in increasing displacements for steady resisting loads. This local mechanism is not replicated by the numerical simulation due to the macro-modelling approach and to the assumption of homogeneous and isotropic masonry. On the other hand, in case of specimen Wall_Tmb, the post-peak numerical branch is slightly closer to the post-peak descending branch of experimental envelop. In this case, the numerical models simulated with higher accuracy the experimental behaviour due to absence of important local resisting mechanisms.

The maximum load achieved in numerical model of Wall_Ref (45.04 kN) is extremely close to the experimental load detected (45.64 kN). The maximum load of about 81.43kN achieved in the numerical model Wall_Stl is about 16% higher if compared to the experimental lateral resistance (69.91 kN). On the other hand, the maximum load obtained in Wall_Ref (67.50 kN) is only 2% lower than the experimental lateral resistance (68.91 kN). These differences can be explained by the possible local resisting mechanism developed in the experimental tests and, additionally, by uncertainties of the effective contact area between the airbag and the wall, as well as by cyclic stiffness and strength degradation occurred during the experimental tests, which was not considered in the numerical analysis.

It should be noted that Figure 23b and c also includes the numerical pushover curves obtained for Wall_Stl and Wall_Tmb considering the material properties for each wall shown in

Table 7, but no reinforcement. These analyses are intended to show how the response of the building is very similar for all three walls with different properties and no reinforcement. Therefore, the analyses confirm that the reinforcement techniques considered have a significant influence on the out-of-plane behaviour of the stone masonry walls analysed.

Figure 24 presents the out-of-plane displacements along Y axis (defined as TDty, according to the convention used in DIANA software) for the tree numerical models (Wall_Ref, Wall_Stl and Wall_Tmb). The numerical models provide a symmetric displacement pattern, as the macro-model, in fact, is not able to replicate all those irregularities characterizing the masonry bond and real interaction among stone units, having different shapes and sizes, and mortar units. However, it can be said that the numerical displacements patterns represent reasonably well he experimental displacements contour maps. As expected, the highest level of displacements was reached in the upper part of the mid-span of the front wall.

Figure 25 presents the maximum principal strains (defined as E1, according to the convention used in DIANA software) for all the tested walls. The figure shows areas of the wall where cracks are most likely to develop. The highest values of strain can be, in fact associated to the development of cracks. It must be pointed out that the images depicting strains distribution are related to a level of displacement equal to 40 mm.

Numerical displacements (m) Experimental displacements (mm)

Preprint version, Reference: Murano, A., Ortega, J., Vasconcelos, G., Rodrigues, H. Influence of traditional earthquake-resistant techniques on the out-of-plane behavior of stone masonry walls: experimental and numerical assessment. *Engineering Structures* (2020). https://doi.org/10.1016/j.engstruct.2019.109815

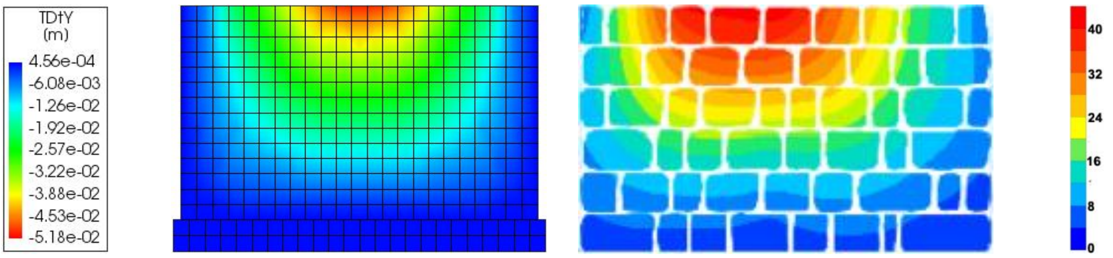

Wall_Ref

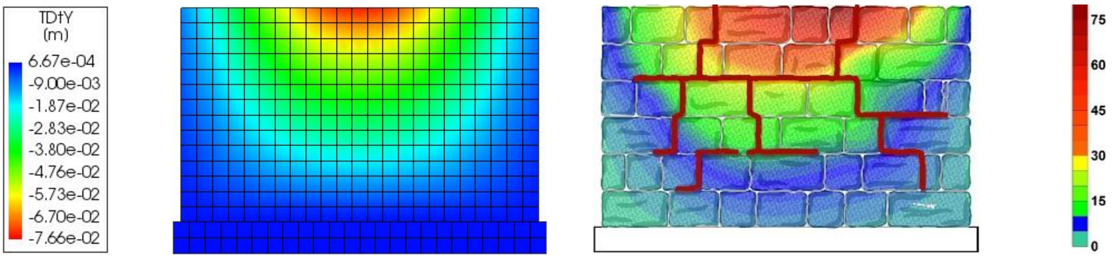

Wall_Stl

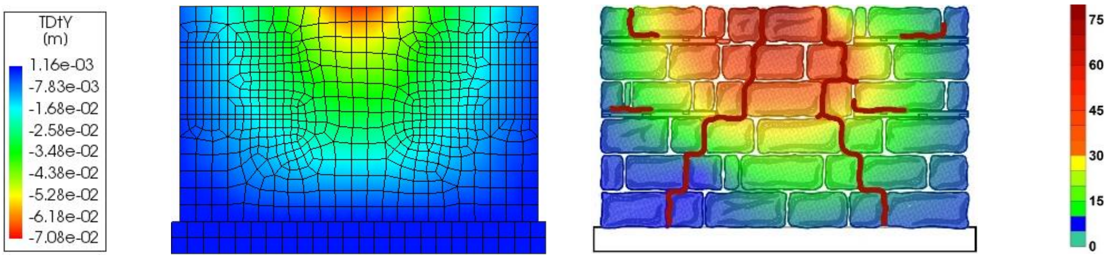

Wall_Tmb

Figure 24 – Displacement contour maps (Numerical vs Experimental)

<u>According to the numerical results, the displacements fields in the frontal wall are compatible with a span supported in three edges. Consequently, the top mid-span part of the frontal wall experienced the highest displacement levels and it is more prone to the bending failure of the walls.</u> Significant strain levels can be also detected in the intersections between frontal and transversal walls, showing the formation of cracks that can eventually lead to the separation of the walls. This phenomenon is important in the reference wall (Wall_Ref), whereas a reduction in terms of strain concentration is visible in Wall_Stl and Wall_Tmb, which is attributed the presence of the reinforcements. Moreover, looking at the model Wall_Tmb, it is possible to notice a high level of deformation at the interface between timber elements and mortar joints. This trend is also confirmed by the crack pattern detected after the out-of-plane test (see Figure 24).

Preprint version, Reference: Murano, A., Ortega, J., Vasconcelos, G., Rodrigues, H. Influence of traditional earthquake-resistant techniques on the out-of-plane behavior of stone masonry walls: experimental and numerical assessment. *Engineering Structures* (2020). https://doi.org/10.1016/j.engstruct.2019.109815

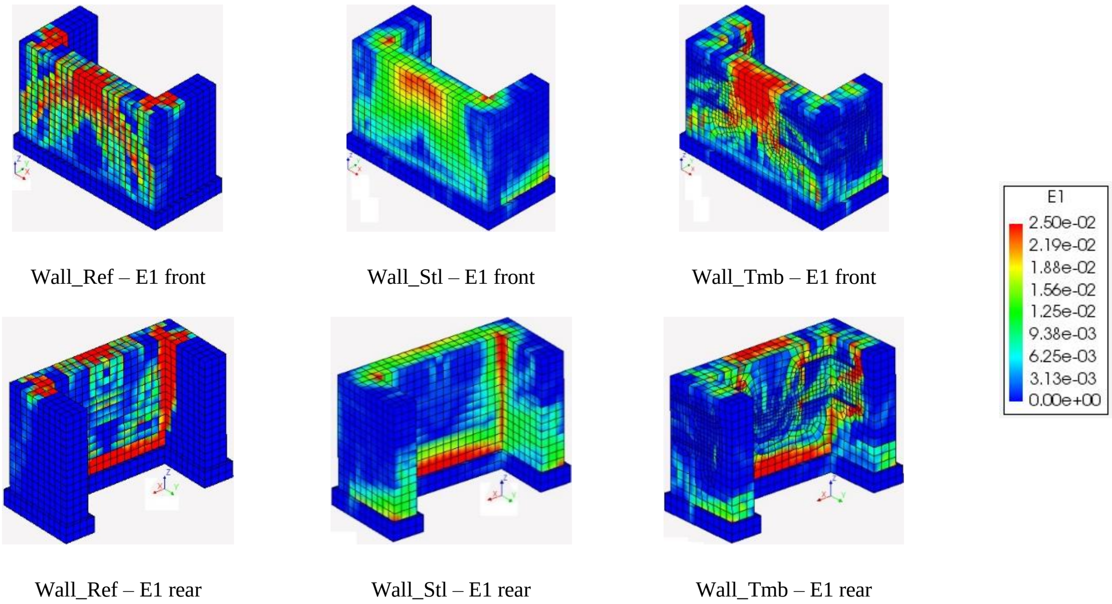

Figure 25 – Maximum principal strain distribution (E1)

Finally, damage is also widespread at the connection between the walls and the concrete base, showing the eventual separation of the walls at the base followed by the out-of-plane rotation of the wall. It should be noted that during the experimental tests, the damage pattern at the inner side of the walls could not be observed. Thus, some cracks, such as those at the base, may be closed and hidden at the end of the test, due to the self-weight of the structure.

Figure 26 overlaps the crack patterns over the maximum principal strains obtained from the numerical analyses. Despite the modelling limitations and the visual limitations during the experiment, the areas of higher concentration of tensile strains are rather consistent with the crack pattern observed in the inner and outer side of the frontal wall, as well as with the cracks observed at the intersection between orthogonal walls after the test. The experimental crack pattern in the unreinforced wall is quite asymmetric.

On the other hand, looking at the crack distribution in the reinforced experimental models, the connectivity exerted by the reinforcing elements is clearly visible. Even if specimen Wall_Stl shows an experimental crack pattern affected by a local mechanism developed at a central portion of the façade, the symmetric distribution of the damages can be considered an evidence and it is consistent with the numerical simulation (Figure 26). The same is valid for the model Wall_Tmb. In this case, the experimental damage distribution is governed by the timber elements configuration, which led to the formation of cracks in the interfaces between timber elements and mortar joints. Moreover, inclined symmetric cracks, developed in the front wall, affect only a reduced portion of façade delimited by the timber elements, showing a good agreement with the numerical strain distribution (Figure 26).

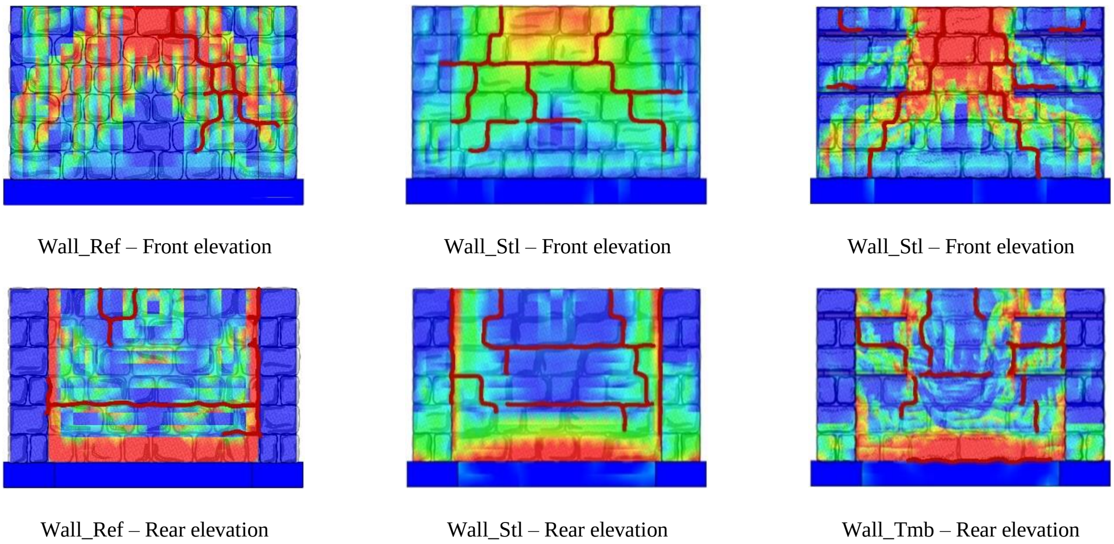

Figure 26 – Overlapping of experimental crack pattern reinforced over the numerical strain distribution

5.4. Parametric study

A parametric study was performed in order to investigate the influence of the configuration, location and number of reinforcing elements (steel and timber-laced) on the out-of-plane behaviour of stone masonry walls. Nevertheless, in order to proceed with a numerical parametric study, firstly it was decided to scale the previously analysed model to real scale.

5.4.1. Analysis of full scale models

For this first analysis, the dimensions of the reduced scale (1:2) experimental models Wall_Ref, Wall_Stl and Wall_Tmb were doubled. Reference scale factors were considered according to the Cauchy law [21]. The material properties were considered the same experimental models as this is a principle of the Cauchy law (same stress). The variation of the scale resulted in a peak load equal to 176.42 kN, 300.80 kN and 262.80 kN in Wall_Ref, Wall_Stl and Wall_Tmb respectively, which is approximately 4 times higher than the experimental value (Figure 27). This result is in agreement with the Cauchy scale factors ($\lambda_F^2 = 4$).

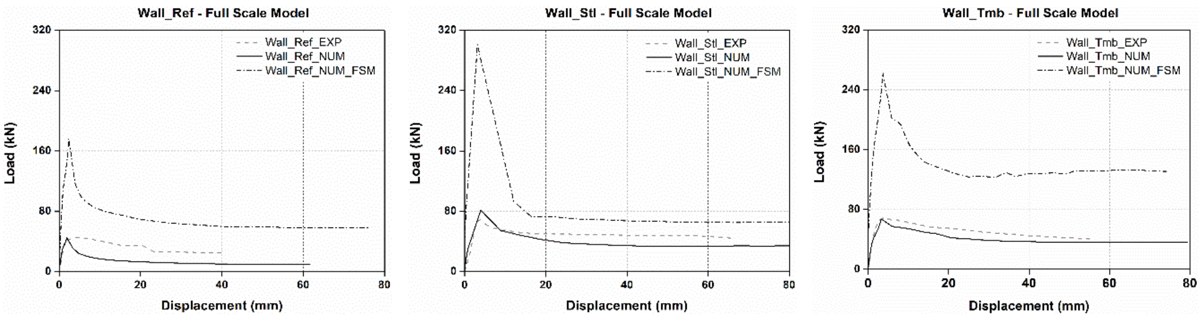

a b c

Figure 27 – Numerical force vs displacement curves for full scale models: Wall_Ref (a), Wall_Stl (b), Wall_Tmb (c)

Figure 28 shows the results in terms of maximum principal strain distribution (E1) in the full-scale models (FSM). According to the correlation between displacement values provided by the Cauchy law, the displacement in the full-scale model (2:1) should double the displacement of the reference model. Therefore, the strain distributions presented in Figure 28 are related to a displacement level equal to 80 mm, whereas in the reduced scale models (RSM) the strain distributions are related to a displacement level equal to 40 mm (see Figure 25 and Figure 26).

It is seen that the strains distributions obtained in the full-scale models is consistent with the results obtained in the reduced scale specimens. Strain concentration is higher in the plain wall (Wall_Ref), mainly in the façade and in the intersection between front and lateral walls. The use of reinforcing elements (steel ties in Wall_Stl and timber-laced reinforcements in Wall_Tmb) contributed to efficiently achieve a reduction in terms of strain distribution in the aforementioned critical areas of the stone masonry walls, similarly to what happens in the reduced scale models.

Preprint version, Reference: Murano, A., Ortega, J., Vasconcelos, G., Rodrigues, H. Influence of traditional earthquake-resistant techniques on the out-of-plane behavior of stone masonry walls: experimental and numerical assessment. *Engineering Structures* (2020). https://doi.org/10.1016/j.engstruct.2019.109815

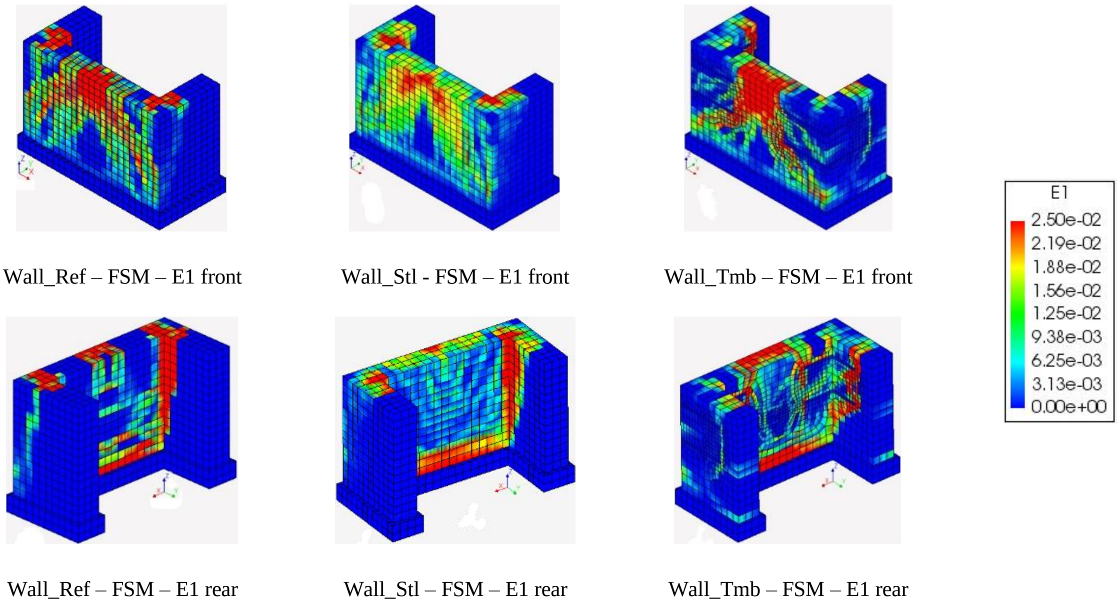

Figure 28 – Maximum principal strain distribution full scale models (E1)

5.4.2. Analysis of reinforcement configuration

The parametric study focus mainly on the analysis of the configuration of the reinforcing steel bars and timber laced elements regarding the location along the height of the walls. The full-scale numerical models were used to carry out the numerical parametric analysis. Therefore, nine numerical models were built varying the geometrical configuration and number of reinforcing elements for each masonry course (Figure 29).

The standard configuration of reinforcements in full scale specimens corresponds to the same as the one considered in the experimental models with the update of the dimensions to real scale. In case of steel reinforcements (Wall_Stl), the number of steel ties in each masonry course has been gradually increased resulting in three different configurations, namely 1A (2 reinforcements in each lateral wall – reference configuration), 1B (3 reinforcements in each lateral wall) and 1C (5 reinforcements in each lateral wall). The same criterion has been applied to full scale model Wall_Tmb. Additionally, a variation in terms of geometry has been applied to the timber-laced reinforcements in model Wall_Tmb, resulting in three models characterized by reinforcing elements that run continuously along the length of the wall arranged in horizontal planes (ring beams or bond beams), see Figure 29. Successively, the number of ring beams

Preprint version, Reference: Murano, A., Ortega, J., Vasconcelos, G., Rodrigues, H. Influence of traditional earthquake-resistant techniques on the out-of-plane behavior of stone masonry walls: experimental and numerical assessment. *Engineering Structures* (2020). https://doi.org/10.1016/j.engstruct.2019.109815

in each masonry course has been increased resulting in configuration 2A (2 reinforcements lying in course 3 and 5 respectively), 2B (3 reinforcements lying in course 1, 3 and 5 respectively) and 2C (a ring beam for each masonry course). For the numerical nonlinear analysis, the reference mechanical properties adopted for Wall_Tmb were assumed for all models.

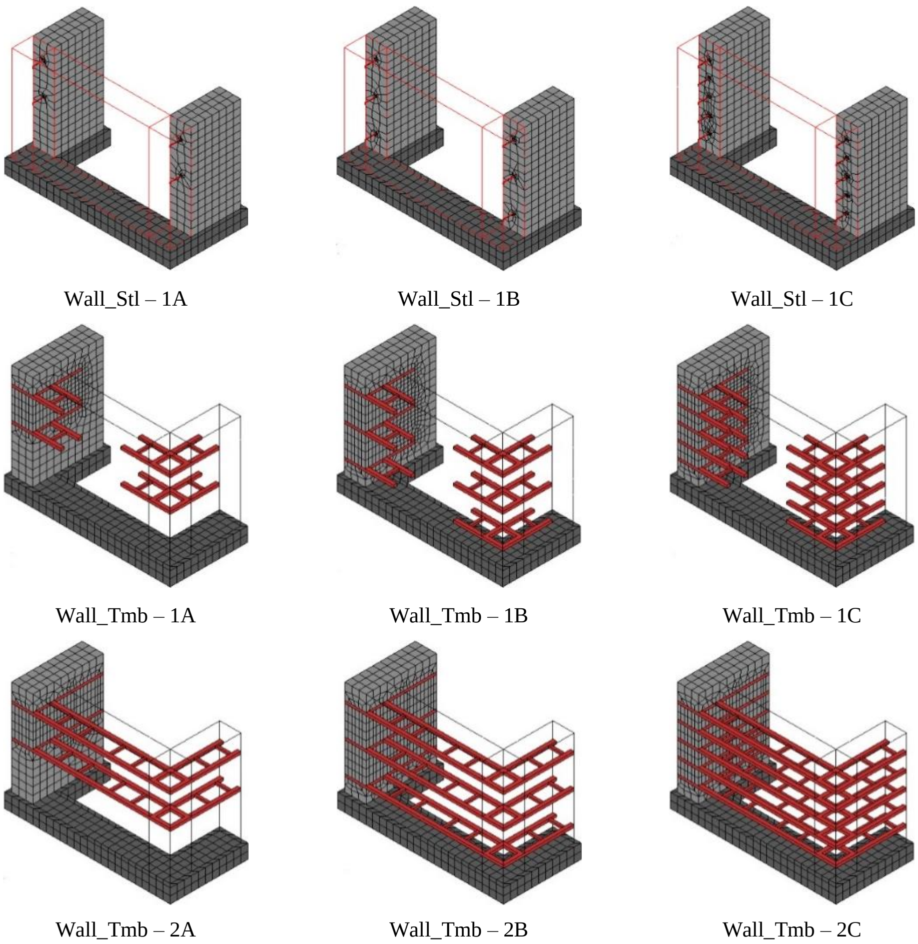

Figure 29 – Variation on the configuration of reinforcements

Figure 30 shows the numerical capacity curves together with the load-displacement diagram of full-the reference scale numerical model (Wall_Ref). The pushover curve obtained for model Wall_Stl highlight a mostly linear elastic behaviour up to the peak load in all reinforcing configurations (1A, 1B and 1C). The post peak branch is characterized by a considerable descending trend after reaching a steady residual load for increasing displacements (Figure 30-a). An increase of the peak load of about 70% was achieved in case of Wall_Stl-1A and Wall_Stl-1B when compared to the peak load obtained in the reference full scale model (Wall_Ref-FSM). In addition, it is also possible to notice that the maximum load in Wall_Stl-1C doubled compared to Wall_Ref_FSM (353.58 kN against 176.42 kN). It is noted that Wall_Stl-1C presents an enhancement of the post-peak performance, with higher levels of residual resistance when compared to models 1A and 1B and Wall_Ref-FSM, which present approximately the same residual post peak load (averagely 160 kN against 60 kN).

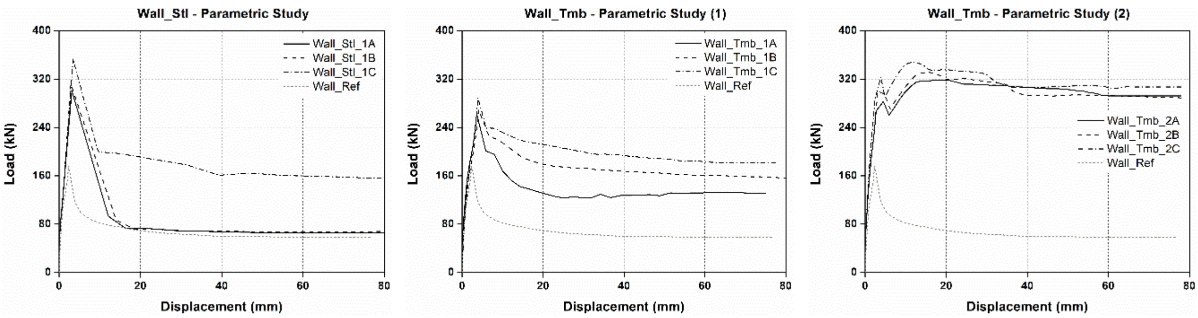

a b c

Figure 30 – Parametric Study: Wall_Stl-1A/1B/1C (a); Wall_Tmb-1A/1B/1C (b) and Wall_Tmb-2A2B/2C (c)

Regarding the wall reinforced with timber laced reinforcement, the peak-load in Wall_Tmb-1A (ca. 262 kN), Wall_Tmb-1B (ca. 268 kN) and Wall_Tmb-1C (ca. 289 kN) are approximately 48%, 52% and 64% respectively higher when compared to Wall_Ref-FSM (ca. 176 kN). The increased number of reinforcements influences the post-peak performance of the walls, resulting in the gradual increment of the residual load levels when compared to the residual post peak load of reference wall Wall_Ref-FSM (averagely 130, 155 and 185 kN in 1A, 1B and 1C configuration respectively against 60 kN in Wall_Ref_FSM).

It is also observed that the length of the timber laced reinforcement (Wall_Tmb-2A/2B/2C) has a great influence in the peak and post peak response of the reinforced walls. The peak load increases by 80% in Wall_Tmb-2A/2B when compared to Wall_Ref-FSM, whereas peak load attained in wall Wall Tmb-2C represent an increase of more than 100% when compared to the unreinforced model (averagely 318, 330 and 348 kN in 2A, 2B and 2C peak load respectively against 160 kN in Wall_Ref_FSM). In addition, the post peak is characterized by a plateau with high values of residyal strength, revealing the great gain in ductility of the specimens. If fact, the walls almost keep the maximum load for increasing post peak displacements. It stressed that the increase in the number of timber ring beams does not reflect important changes in the peak load and particularly in the post peak branch.

In general, the addition of reinforcements at the first masonry course does not result in a considerable improvement of the wall structural capacity in terms of peak load. An increase of about 4% in the peak load was recorded in case of steel reinforcements. This is explained by the deformation patterns of the walls, which exhibit low levels of displacement (strains) close to the bottom fixed boundary, leading to reduced effectiveness of the reinforcements. This also justify the higher effectiveness of reinforcements at the uppers courses, because, at these levels the strains developed at the reinforcements should be higher and thus more active. They result in the increase of attained peak load and in a reduction of the strain concentration in the upper part of masonry wall. This trend manly characterizes the results related to 1B and 1C configuration.

The additional number of reinforcing elements enhances the monolithic behaviour of the U-shaped plan walls by improving the connection levels between the façade and transversal walls. This is clearly visible in the maximum principal strain distribution in configuration C (Figure 31, Figure 32 and Figure 33). The failure mode obtained for all walls consists of a rocking mechanism and overturning of the wall with respect to the base, instead of the higher trend of separation of the façade walls from the transversal walls. In models Wall-Stl (1B and 1A) (Figure 31), the extension of high levels of strains at the vertical connections and bottom base is considerably higher than the extension of maximum strains developed in model 1C. On the other hand, the tensile strains at the mid-span top region reduces considerable in the later model when compared to Wall-Stl 1A and Wall-Stl 1B.

Preprint version, Reference: Murano, A., Ortega, J., Vasconcelos, G., Rodrigues, H. Influence of traditional earthquake-resistant techniques on the out-of-plane behavior of stone masonry walls: experimental and numerical assessment. *Engineering Structures* (2020). https://doi.org/10.1016/j.engstruct.2019.109815

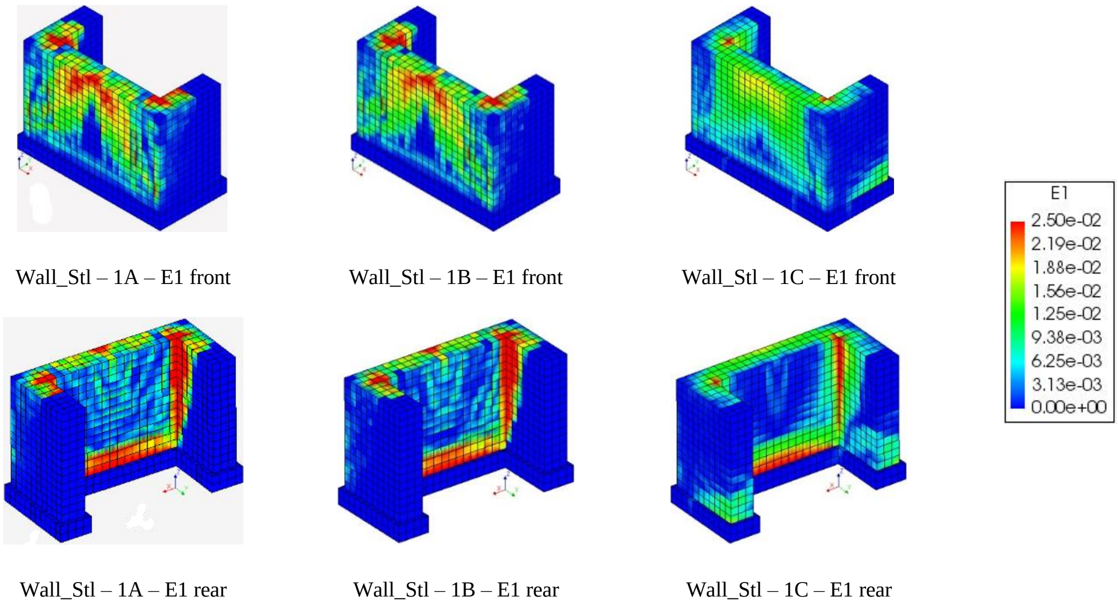

Figure 31 – Wall_Stl maximum principal strain distribution (1A, 1B, 1C) at 80 mm displacement

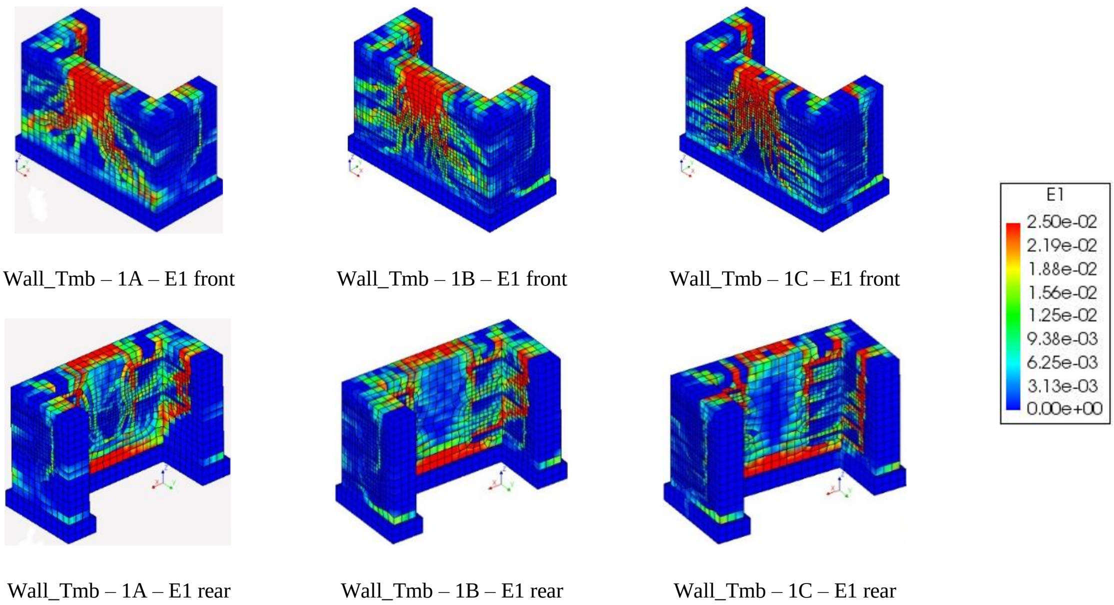

Figure 32 – Wall_Tmb maximum principal strain distribution (1A, 1B, 1C) at 80 mm displacement

The addition of the so-called ring beams resulted in a significant improvement of the monolithic behaviour of the walls with the different geometric configurations (2A, 2B and 2C). It should be noted that when the number of ring beams within the walls increases, the strains are progressively decreasing in the walls (from 2A to 2C configuration), being the strain concentration transferred to the bottom part of the wall, promoting the development of global rocking mechanism, see Figure 33. This behaviour is also responsible for the higher ductility of the masonry walls, reflected in the post peak plateau of the force-displacement diagrams previously analysed (Figure 30-c). Finally, it is stressed that the increase in the number of timber ring beams does not result in a significant enhancement of the walls, meaning that the reference configuration (timber ring beams close to the top of the walls) is enough to ensure the improvement of the stone masonry walls by promoting the monolithic behaviour.

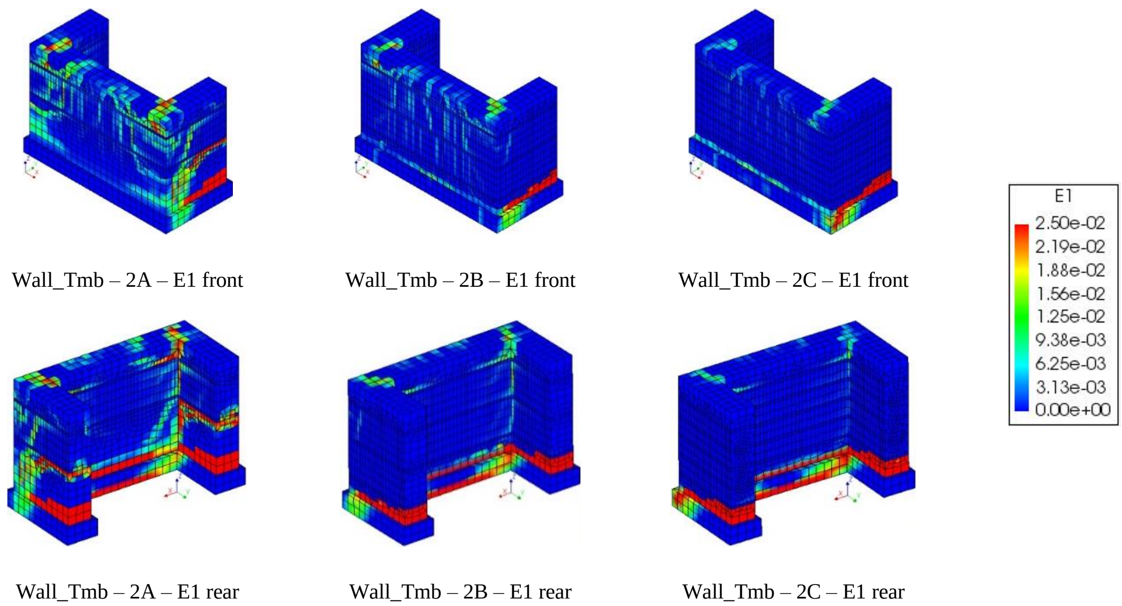

Figure 33 – Wall_Tmb maximum principal strain distribution (2A, 2B, 2C) at 80 mm displacement

6. Conclusions

This paper presents the results of the experimental and numerical characterization of the out-of-plane behaviour of two U-shaped plan configuration stone masonry walls built with two different earthquake-resistant techniques, namely steel ties and timber laced reinforcement placed embedded at the corners of the walls. Both techniques aimed at the improvement of the connection between the façade and transversal walls. The results are systematically compared with the response of an unreinforced walls with the same geometric and morphologic features and tested using the same setup and procedure. The systematic comparison enabled the discussion on the performance of the strengthening techniques regarding out-of-plane loading.

The experimental characterization included non-destructive tests, namely sonic and dynamic identification tests, intending to estimate the mechanical elastic properties of the masonry. The characterization of the out-of-plane behaviour of the stone masonry walls was carried out through quasi-static out-of-plane loading tests performed using an airbag to apply a uniform horizontal load that simulate the seismic action. The experimental out-of-plane response was characterized by an almost linear behaviour until the peak load was reached. The post peak behaviour in the wall reinforced with steel ties was characterized by softening branch stabilizing in residual resistance close to the residual resistance of reference unreinforced masonry wall. This trend was mainly related to a local resisting mechanism characterized by sliding of the mid-span top part of the wall. On the other hand, the unreinforced wall and the wall reinforced with timber laced reinforcement showed a relatively smooth softening in the post-peak branch, characterized by a decrease of the force for increasing lateral displacements. The maximum load obtained in both reinforced walls was slightly below 70 kN, which represented a significant improvement of about 45% when compared with the unreinforced wall. Moreover, the presence of the reinforcing elements resulted in a more symmetric crack pattern and contributed, at the same time, to reduce the damage concentration at the connection with the transversal walls of the specimens.

A numerical nonlinear analysis was also carried out in order to assess the influence of the arrangement of reinforcement in the out-of-plane response of the stone masonry walls. For this, a macro-modelling approach was followed, assuming the stone masonry as a homogenous and isotropic material. The numerical model was previously calibrated based on results of non-destructive tests (sonic and dynamic identification tests) and on the force vs displacement curves resulting from out-of-plane tests. The numerical model proved to be calibrated as the pushover curves obtained from the numerical analysis showed a good correlation with the experimental force-displacement envelopes. A good correlation was also obtained in terms of maximum load capacity, stiffness, deformation and damage pattern.

The outcomes of the parametric study showed that the presence of reinforced elements, particularly close to the top of the wall, has a major role in the out-of-plane performance of the walls but it was seen that increasing the number of reinforcing elements does not result in a significant improvement of the structural response in terms of maximum load attained, but contribute for the improvement of monolithic behaviour and ductility. This is particularly relevant in case of timber ring beams, whose confining effect results in a predominant rock behaviour of the structure.

To conclude, this work highlights the importance of a good experimental characterization of stone masonry walls to correctly understand their structural behaviour. This characterization is important to later develop reliable numerical models from which better understanding on the structural behaviour can be achieved. The results provided in this work also contribute to understand the efficiency of traditional earthquake resistant techniques on improving the out-of-plane behaviour of stone masonry walls and it is also a valuable contribution in order to foster the reintroduction of these techniques in engineering conservation practice aiming at the preservation of vernacular architecture. Loss of knowledge on traditional materials and construction techniques has often led to the demolition and reconstruction of buildings based on modern materials and up-to-date design approaches. This is the reason why, recovering a renewed awareness of using traditional construction techniques can be considered a starting point in preventing the abandonment of vernacular buildings that are many times considered unsafe avoiding, at the same time, an inestimable loss of heritage value.

7. Acknowledgments

The authors would like to acknowledge the important collaboration of the company *Fassa Bortolo Portugal* by providing the mortar for the construction of experimental specimens.

References

[1] J. Ortega, *PhD Thesis,* Guimaraes: University of Minho, 2018.

[2] A. Giuffrè, Sicurezza e conservazione dei centri storici - Il caso Ortigia, A. Giuffrè, Ed., Bari: Editori Laterza, 1993.

[3] B. Helly, “Local seismic cultures: a European research program for the protection of traditional housing stock,” *Annals of Geophysics,* pp. 791-794, November-December 1995.

[4] J. Ortega, G. Vasconcelos, H. Rodrigues and M. Correia, “Local Seismic Cultures: The use of timber frame structures in the South of Portugal,” in *2nd International Conference on Historic Earthquake-Resistant Timber Frames in the Mediterranean Region*, Lisbon, 2015.

[5] N. Ruggeri, G. Tampone and R. Zinno, Historical Earthquake-Resistant Timber Frames in the Mediterranean Area, Berlin: Springer, 2015.

[6] E. Vintzileou, “Timber-reinforced structures in Greece: 2500 BC–1900 AD,” *Structures and Buildings,* pp. 167-180, May 2011.

[7] R. Langenbach, “From “Opus Craticium” to the “Chicago Frame”: Earthquake-Resistant Traditional Construction,” *International Journal of Architectural Heritage,* pp. 29-59, May 2007.

[8] M. Tomazevic, Earthquake-Resistant Design of Masonry Buildings, London: Imperial College Press, 1999.

[9] T. M. Ferreira, A. Costa and A. Costa, “Analysis of the Out-Of-Plane Seismic Behavior of Unreinforced Masonry: A Literature Review,” *International Journal of Architectural Heritage,* pp. 949-972, November 2014.

[10] K. T. Doherty, *PhD Thesis,* Adelaide: Department of Civil and Environmental Engineering, 2000.

[11] D. D'Ayala, Y. Shi and C. Stammers, “Dynamic multi-body behaviour of historic masonry buildings models,” in *Structural Analysis of Historic Construction*, London, 2008.

[12] O. Al Shawa, L. Sorrentino and D. Liberatore, “Simulation Of Shake Table Tests on Out-of-Plane Masonry Buildings. Part (II): Combined Finite-Discrete Elements,” *International Journal of Architectural Heritage*, pp. 79-93, November 2016.

[13] A. Costa, A. Arêde, A. Campos Costa, A. Penna and A. Costa, “Out-of-plane behaviour of a full scale stone masonry façade. Part 2: shaking table tests,” *Earthquake Engineering and Structural Dynamics*, p. 2097–2111, June 2013.

[14] Candeias, C. Costa, Mendes, Costa and Lourenço, “Experimental Assessment of the Out-of-Plane Performance of Masonry Buildings Through Shaking Table Tests,” *International Journal of Architectural Heritage*, pp. 31-58, December 2016.

[15] U. Tomassetti, A. Correia, P. Candeias, F. Graziotti and A. Campos Costa, “Two-way bending out-of-plane collapse of a full-scale URM building tested on a shake table,” *Bulletin of Earthquake Engineering*, vol. 17, no. 4, p. 2165–2198, 2018.

[16] F. Graziotti, U. Tomassetti, S. Sharma, L. Grottoli and G. Magenes, “Experimental response of URM single leaf and cavity walls in out-of-plane two-way bending generated by seismic excitation,” *Construction and Building Materials*, vol. 195, pp. 650-670, 2019.

[17] T. M. Ferreira, A. Costa, A. Arede, A. Gomes and A. Costa, “Experimental characterization of the out-of-plane performance of regular stone masonry walls, including test setups and axial load influence,” *Bull Earthquake Eng*, p. 2667–2692, March 2015.

[18] D. Dizhur, H. Derakhshan, R. Lumantarna, J. Ingham and G. M.C., “In-situ out-of-plane testing of unreinforced masonry wall segment in Wintec Block F building,” in *NZSEE Conference*, Auckland, 2010.

[19] J. Vaculik and M. C. Griffith, “Out-of-plane shaketable testing of unreinforced masonry walls in two-way bendin,” *Bulletin of Earthquake Engineering,* vol. 16, no. 7, p. 2839–2876, 2018.

[20] M. Griffith and J. Vakulik, “Out-of-plane flexural strength of unreinforced clay brick masonry walls,” *TMS Journal,* vol. 25, no. 1, pp. 53-68, 2007.

[21] H. Maccarni, G. Vasconcelos, H. Rodrigues, J. Ortega and P. B. Lourenço, “Out-of-plane behavior of stone masonry walls: Experimental and numerical analysis,” *Construction and Building Materials,* pp. 430-452, 2018.

[22] P. Roca, M. Cervera, G. Gariup and L. Pelà, “Structural Analysis of Masonry Historical Constructions - Classical and Advanced Approaches,” *Arch Comput Methods Eng,* 299-325 July 2010.

[23] P. Lourenço, “Recent advances in Masonry modelling: micromodelling and homogenisation,” in *Multiscale Modeling in Solid Mechanics: Computational Approaches*, London, Imperial College Press, 2009, pp. 251-294.

[24] L. Martins, G. Vasconcelos, J. Ortega, P. Lourenço, H. Rodrigue, L. Silva and C. Palha, “Characterization of dry stone walls to out-of plane actions,” in *10th Congresso Nacional de Mecânica Experimental*, Lisbon, 2016.

[25] European Committee for Standardization, *EN 1015-11,* Brussels: CEN, 1999.

[26] G. Vasconcelos, *PhD Thesis,* Guimaraes: University of Minho, 2005.

[27] A. Borri, M. Corradi, G. Castori and A. De Maria, “A method for the analysis and classification of historic masonry,” *Bull Earthquake Eng,* p. 2647–2665, February 2015.

[28] A. Borri and A. De Maria, “Masonry Quality Index (MQI): correlation with the mechanical characteristics and knowledge levels,” *Progettazione Sismica*, pp. 45-63, March 2015.

[29] L. F. Miranda, J. Rio, J. Miranda Guedes and A. Costa, “Sonic Impact Method – A new technique for characterization of stone masonry walls,” *Construction and Building Materials*, pp. 27-35, June 2012.

[30] Á. Cunha and E. Caetano, “From input-output to output-only modal identification of civil engineering structures,” in *1st International Operational Modal Analysis Conference (IOMAC)*, Copenhagen, Denmark, 2005.

[31] N. M. M. Maia and J. M. M. Silva, “Modal analysis identification techniques,” *Philosophical Transactions of the Royal Society A: Mathematical, Physical and Engineering Sciences*, vol. 359, no. 1778, pp. 29-40, 2001.

[32] European Committee for Standardization, *EN 1998-3*, Brussels: CEN, 2005.

[33] M. Tomazevic and P. Weiss, “Seismic behavior of plain and reinforced masonry buildings,” *Journal of Structural Engineering*, pp. 323-338, 1994.

[34] M. Tomazevic and I. Klemenc, “Verification of seismic resistance of confined masonry buildings,” *Earthquake Engineering and Structural Dynamics*, pp. 1073-1088, 1997.

[35] DIANA - Finite Element Analysis , DIsplacement method ANalizer. User's Manual, release 10.2, Delft, The Netherlands: DIANA FEA BV , 2017.

[36] P. B. Lourenço, “Masonry Modeling,” in *Encyclopedia of Earthquake Engineering*, Berlin, Springer Berlin Heidelberg, 2015, pp. 1-13.

[37] P. B. Lourennço and J. M. Pereira, “Seismic Retrofitting Project: Recommendations for Advanced Modeling of Historic Earthen Sites,” The Getty Conservation Institute, Los Angeles, 2018.